Informatics

Deformationsbasierte Visualisierung von Brust-MRT-Aufnahmen in Rückenlage

DIPLOMARBEIT

zur Erlangung des akademischen Grades

Diplom-Ingenieurin

im Rahmen des Studiums

Media and Human-Centered Computing

eingereicht von

Julia Kummer, BSc
Matrikelnummer 51912522

an der Fakultät für Informatik

der Technischen Universität Wien

Betreuung: Associate Prof. Dr.in Renata Raidou
Mitwirkung: Dipl.-Math.in Dr.in Katja Bühler

Wien, 30. Mai 2025

_____   _____
          Julia Kummer   Renata Raidou

Informatics

Flattening-Based Visualization of Supine Breast MRI

DIPLOMA THESIS

submitted in partial fulfillment of the requirements for the degree of

Diplom-Ingenieurin

in

Media and Human-Centered Computing

by

Julia Kummer, BSc

Registration Number 51912522

to the Faculty of Informatics

at the TU Wien

Advisor: Associate Prof. Dr.in Renata Raidou
Assistance: Dipl.-Math.in Dr.in Katja Bühler

Vienna, May 30, 2025 _____ _____
Julia Kummer Renata Raidou

Erklärung zur Verfassung der Arbeit

Julia Kummer, BSc

Hiermit erkläre ich, dass ich diese Arbeit selbständig verfasst habe, dass ich die verwendeten Quellen und Hilfsmittel vollständig angegeben habe und dass ich die Stellen der Arbeit – einschließlich Tabellen, Karten und Abbildungen –, die anderen Werken oder dem Internet im Wortlaut oder dem Sinn nach entnommen sind, auf jeden Fall unter Angabe der Quelle als Entlehnung kenntlich gemacht habe.

Ich erkläre weiters, dass ich mich generativer KI-Tools lediglich als Hilfsmittel bedient habe und in der vorliegenden Arbeit mein gestalterischer Einfluss überwiegt. Im Anhang „Übersicht verwendeter Hilfsmittel“ habe ich alle generativen KI-Tools gelistet, die verwendet wurden, und angegeben, wo und wie sie verwendet wurden. Für Textpassagen, die ohne substantielle Änderungen übernommen wurden, habe ich jeweils die von mir formulierten Eingaben (Prompts) und die verwendete IT-Anwendung mit ihrem Produktnamen und Versionsnummer/Datum angegeben.

Wien, 30. Mai 2025

_____

Julia Kummer

Acknowledgements

First and foremost, I would like to thank my supervisors, Katja Bühler and Renata Raidou, for their invaluable guidance and constructive feedback throughout this thesis. Special thanks also goes to Elmar Laistler and Lena Nohava, part of the MR physics team, for their support, sharing their expertise and also taking the time to participate in the interviews. I am also very grateful to the radiologists of the AKH Wien, whose insights and participation in both the initial interviews and the final evaluation were essential to this work.

Kurzfassung

In dieser Arbeit werden zwei neue Visualisierungsmethoden zur Deformation von Brust-
bildern in Rückenlage vorgestellt. Dabei wird das Brustgewebe „abgeflacht", um die
Untersuchung innerhalb weniger koronaler Schichten zu ermöglichen. Brustkrebs ist die
weltweit am häufigsten diagnostizierte Krebserkrankung bei Frauen. Eine frühzeitige
Erkennung von Läsionen ist entscheidend, um die Sterblichkeitsrate zu senken. Die
Magnetresonanztomographie (MRT) der Brust in Rückenlage ermöglicht eine präzisere
Lokalisierung von Läsionen für bildgeführte Interventionen. Die herkömmliche axiale Vi-
sualisierung ist jedoch suboptimal, da sich das Gewebe entlang der Brustwand ausbreitet
und über zahlreiche Schichten verteilt.

Im Rahmen eines nutzerzentrierten Designprozesses wurden zwei Methoden zur Defor-
mation entwickelt. Die erste Methode, der sogenannte Surface-Cutting-Ansatz, erzeugt
mehrere Meshes, die entlang eines Distance-Fields nach innen versetzt und anschließend
unabhängig voneinander mittels As-Rigid-As-Possible-(ARAP)-Parameterisierung abge-
flacht werden. Die zweite Methode basiert auf einer Verzerrung (Warp), die das gesamte
Brustvolumen in einem Schritt anhand anatomisch definierter Kontrollpunkte deformiert.
Während der Surface-Cutting-Ansatz auf der Parameterisierung einzelner Oberflächen
beruht, nutzt die zweite Methode Kontrollpunkte, um eine zusammenhängende, globale
Deformation zu realisieren.

Die Evaluierung durch Expertinnen und Experten zeigte, dass der Surface-Cutting-Ansatz
einen intuitiven Überblick sowie eine klare Darstellung der Blutgefäße ermöglicht. Zudem
weist die Methode eine geringe Verzerrung in Bezug auf Längen (2,1–3,5%) und Flächen
(3,7–5,8%) auf. Durch die unabhängige Parametrisierung einzelner versetzter Oberflä-
chen können jedoch Verzerrungen zwischen den abgeflachten Bildschichten auftreten.
Die zweite Methode gewährleistet eine kontinuierliche volumetrische Parametrisierung
der Schichten und unterstützt direkte Annotationen und Messungen. Radiologinnen
und Radiologen präferierten diese Methode bei der Inspektion von Läsionen aufgrund
der höheren anatomischen Genauigkeit. Beide Ansätze führten zu einer signifikanten
Reduktion der Bildschichten, was ein großes Potenzial zur Zeitersparnis aufzeigt — ein
entscheidender Faktor für die klinische Akzeptanz von Brust-MRTs in Rückenlage.

Abstract

We propose two novel visualization methods optimized for supine breast images that "flatten" breast tissue, facilitating examination of larger tissue areas within each coronal slice. Breast cancer is the most frequently diagnosed cancer in women, and early lesion detection is crucial for reducing mortality. Supine breast magnetic resonance imaging (MRI) enables better lesion localization for image-guided interventions; however, traditional axial visualization is suboptimal because the tissue spreads over the chest wall, resulting in numerous fragmented slices that radiologists must scroll through during standard interpretation.

Using a human-centered design approach, we incorporated user and expert feedback throughout the co-design and evaluation stages of our flattening methods. Our first proposed method, a *surface-cutting* approach, generates offset surfaces and flattens them independently using As-Rigid-As-Possible (ARAP) surface mesh parameterization. The second method uses a *landmark-based warp* to flatten the entire breast volume at once. While the surface-cutting approach is based on the parameterization of individual surfaces, the second method uses control points to realize a coherent, global deformation.

Expert evaluations revealed that the surface-cutting method provides intuitive overviews and clear vascular detail, with low metric (2.1–3.5%) and area (3.7–5.8%) distortions. However, independent slice flattening can introduce depth distortions across layers. The landmark warp offers consistent slice alignment and supports direct annotations and measurements, with radiologists favoring it for its anatomical accuracy. Both methods significantly reduced the number of slices needed to review, highlighting their potential for time savings and clinical impact — an essential factor for adopting supine breast MRI.

Contents

CHAPTER 1

Introduction

This chapter introduces the thesis by outlining the motivation, problem statement, research objectives, and structure of the work.

1.1 Motivation and Problem Definition

Breast cancer is the most frequently diagnosed malignant disease among women worldwide [62]. In order to reduce breast cancer mortality, early lesion detection is of high importance [26]. In this context, medical imaging plays an important role in facilitating timely diagnosis and treatment [26]. While X-ray mammography (XRM) is the standard screening procedure for breast imaging, magnetic resonance imaging (MRI) offers distinct advantages, including better soft tissue contrast and high sensitivity independent of breast density. Additionally, unlike XRM, MRI scans do not require ionizing radiation [52]. In particular, contrast-enhanced breast MRI is very effective in lesion characterization and early cancer detection [52]. Recent studies suggest that imaging in the supine position, in which the patient lies face-up, may further improve lesion localization and support more precise biopsy and surgical planning [41].

Despite these advantages, the complexity of medical images can present challenges in the interpretation and analysis. For example, multiple datasets must be integrated and the high resolution often results in longer inspection times. Additionally, due to the 3D nature of MRI, analysis often requires inspection from different anatomical views [33], typically examined slice by slice in coronal, axial, and sagittal orientations [34]. The complexity increases with supine breast MRIs, where traditional axial views are suboptimal due to the spread of breast tissue over the chest wall. Therefore, existing methods of visualization may not fully support the efficient detection and diagnosis of lesions [43].

To address similar challenges, visualization techniques often rely on parameterization strategies that project (or "flatten") 3D data into 2D representations. Flattening methods

have been successfully developed for analyzing various anatomical structures, including the circulatory system, colon, brain, tumors, and bones [33, 50]. Such techniques are identified in medical visualization as effective means for improved human readability. By leveraging the characteristics of human spatial perception, they reduce the cognitive load of tasks like diagnosis and comparison, making them less cognitively demanding for radiologists [28, 50]. One example is the assessment of rib bone lesions, which often requires findings to be assigned to specific ribs. Using standard views (see Figure 1.1, upper row), this task can be tedious and error-prone since radiologists must track detections back to the corresponding backbone segment. Flattened views aim at providing a more condensed overview of the rib cage and facilitate a faster and more accurate assessment [34].
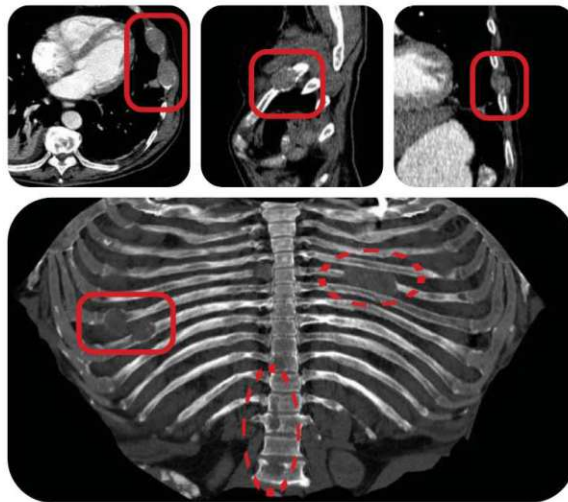

Figure 1.1: Rib cage with tumors. Upper row: standard axial, sagittal, and coronal views. Lower row: flattened slice, showing whole structure. Lesions marked by solid boxes appear in both views; dotted boxes highlight additional pathologies visible only in the flat view (from [34]).

For supine breast MRI, flattened representations can significantly reduce the number of slices a radiologist needs to review, offering potential time savings [43]. While many flattening techniques focus on 2D parameterizations — such as projecting the brain surface onto a plane [50] — breast MRI requires the preservation of the full 3D breast structure. This supports interpretation of the entire breast volume while still allowing conventional slice-by-slice examination.

The goal of this thesis is to develop and evaluate a flattened volumetric breast visualization method specifically tailored to supine MRI. The new visualizations do not aim at replacing standard breast MRI views but rather serve as an initial overview, that allows radiologists to examine larger breast tissue areas per slice, enhancing the utility of supine breast MRI in clinical practice.

1.2 Aim of the work

To what extent can a flattening-based visualization method improve the clinical utility of supine breast MRI?

To address this question, our work first reviews the state-of-the-art in flattening-based visualization techniques and examines how such methods can be adapted to the context of breast MRI. We explore the diagnostic workflows of radiologists, identifying the specific needs and requirements for effective lesion detection in supine breast MRI. Building on these insights, interactive visualization prototypes are designed and implemented. These prototypes incorporate the needs of radiologists, support exploration of different flattening strategies, and maintain spatial correspondence between flattened and original image representations. Finally, the effectiveness of these prototypes was assessed in a user-centered evaluation, focusing on their utility in a diagnostic process.

The main contribution of this thesis is the development of two novel flattening-based visualizations for supine breast MRI. These visualizations present larger areas of breast tissue per slice and aim at improving the clinical utility of supine breast MRI.

1.3 Outline of the Thesis

The chapters of this work are structured in the following way: Chapter 2 will explain the medical background around breast anatomy, breast cancer and the involved imaging techniques, with a focus on breast MRI. In Chapter 3, we cover the current state of the art in flattening based medical visualizations. Chapter 4 summarizes the user requirements for a new visualization, discussed with radiologists and medical physics experts. Based on these requirements, focus of Chapter 5 is how we approached the design of the new visualization, including the deformation techniques that were applied for the prototypes. Following that, we describe the concrete implementation details of the prototypes in Chapter 6. Chapter 7, then delves into the Evaluation, including quantitative evaluation of distortion as well as qualitative feedback obtained from user interviews. Finally, the thesis is concluded in Chapter 8, which summarizes the findings and discusses directions for future work.

Clinical Background

This section provides an overview of the medical background relevant for this work, focusing on breast cancer and the procedures used in breast imaging.

2.1 Anatomy of the Breast

Figure 2.1 illustrates the anatomy of the breast.It consists of lobes, lobules, and ducts. Each breast has 15 to 20 lobes, which contain smaller lobules that produce milk. These lobules are connected by ducts, which carry the milk to the nipple [44]. The breast mainly consists of adipose and glandular tissue, with connective tissue providing structural support. Anatomically, it extends from the second to the sixth rib and reaches into the axilla (armpit), where glandular tissue continues beyond the main breast area. This region is clinically significant, as malignant masses may develop in the axillary extension. The breast lacks muscle but contains lymph nodes, blood vessels, and lymph vessels. The pectoral muscle lies beneath it, separating it from the ribcage [25].

2.2 Breast Cancer

Breast cancer occurs when abnormal breast cells grow uncontrollably and form tumors. These cancerous cells typically form inside the milk-producing lobules and/or the ducts of the breast [2]. The axillary region can play a crucial role in the spread of the disease. The cancer can remain localized or invade nearby tissue, leading to tumor formation and potential metastasis, which can be life-threatening [2, 25].

While specific risk factors exist, approximately half of breast cancer cases occur in women with no identifiable risk beyond sex and age. It is the most common cancer in women across 157 countries and was responsible for 670,000 deaths globally in 2022 [2]. Early detection through medical imaging is crucial for reducing mortality [25, 43].
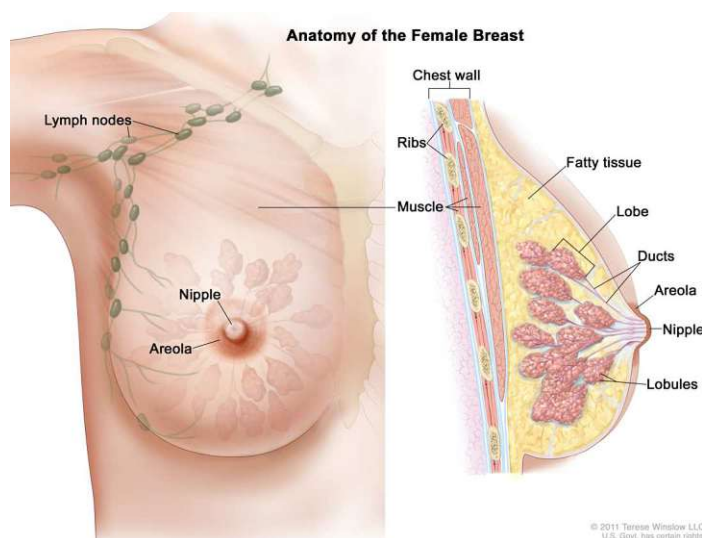
Figure 2.1: Anatomy of the female breast. Illustration by Terese Winslow, used with permission (from [44]).

2.3 Breast Imaging Techniques

This section will discuss the main breast imaging techniques used in clinical practice.

2.3.1 Mammography

XRM is the gold standard for breast cancer screening and relies on mechanical compression of the breast to generate 2D images from 3D tissue [25, 44]. As an optical method, mammography exposes the breast to an X-ray beam, capturing a 2D projection of the internal tissue distribution. Glandular and adipose tissues can be differentiated based on their varying water concentrations, which result in differences in brightness [25].

However, mammography has limitations, especially in certain groups of patients. It is less effective for younger subjects, because they are more likely to have dense breast tissue. Both tumors and dense tissue appear white on mammograms, making it difficult to distinguish between them [44]. Therefore, the sensitivity of mammography significantly decreases in dense breasts, sometimes even resulting in an oversight of invasive cancers [52]. Additionally, it is less sensitive to small tumors, particularly those smaller than 1 mm, which may remain undetected [69]. In cases where mammography is insufficient, other imaging techniques, such as MRI or ultrasound, are used to provide further clarification [25].

2.3.2 Breast Sonography

Breast sonography is an ultrasound procedure and therefore employs high-frequency sound waves to create images of internal breast tissue. It serves as a complementary tool

to XRM, helping to differentiate between cysts and solid masses and guiding biopsies when needed [53]. This method is employed for individuals at high risk for breast cancer, pregnant women and individuals unable to undergo mammography [69]. While ultrasound improves cancer detection in certain cases, it has limitations, such as lower efficiency compared to mammography and difficulty distinguishing between healthy and cancerous tissue due to similar acoustic properties. Additionally, its accuracy depends heavily on the experience of the radiologist [69].

2.3.3 Breast MRI

Breast MRI is a noninvasive imaging modality that utilizes a strong magnetic field and radio-frequency (RF) pulses to generate three-dimensional images of breast tissue [44]. It creates very detailed images and is in addition to mammography and ultrasound for breast cancer screening, staging, and monitoring treatment response, particularly in high-risk patients or those with dense breast tissue [38, 45]. As described above, XRM is the standard screening tool, but MRI offers superior soft tissue contrast and higher sensitivity, making it especially useful in complex cases where other imaging techniques do not provide conclusive results [27, 52]. Additionally, unlike XRM, MRI scans do not require ionizing radiation [52]. The procedure is performed with the patient lying in the prone position, with breasts hanging in dedicated cup-shaped molds of RF coils as illustrated in Figure 2.2.

MRI of the Breast

© 2022 Terese Winslow LLC
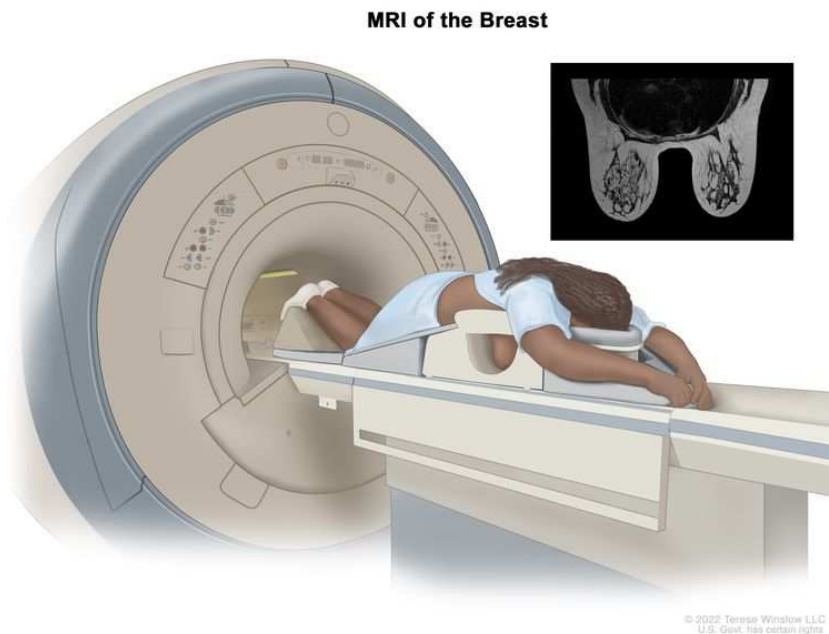U.S. Govt. has certain rights

Figure 2.2: Prone MRI acquisition with breasts positioned in dedicated cup-shaped molds of RF coils. Illustration by Terese Winslow, used with permission (from [44]).

Multiplanar Reconstruction

Unlike mammography, which produces a two-dimensional projection, breast MRI captures the entire breast as stacks of tomographic slices, with each slice typically being a millimeter thick. The volumetric representation enables the reconstruction of two-dimensional sections in standard anatomical orientations — sagittal, coronal, and axial — as well as, when needed, oblique planes [48, 52]. Collectively, these standard axial, sagittal, and coronal planes are referred to as orthogonal views. Figure 2.3 illustrates these common orientations: the sagittal plane divides the body into left and right side, the coronal (or frontal) plane separates front from back, and the axial (or transverse) plane slices the body into upper and lower sections. Images resulting from the axial plane are often referred to as "cross sections" [9].
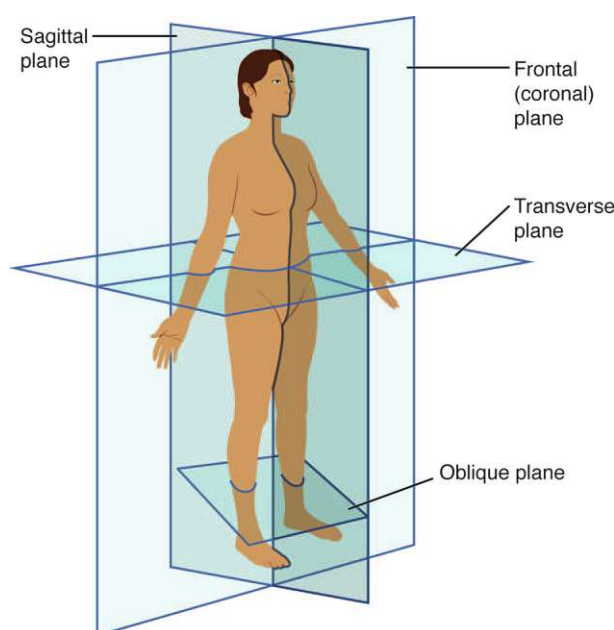

Figure 2.3: Anatomical planes of the human body: sagittal, coronal, and axial (transverse) orientations (from [9]).

This multi-planar reconstruction is crucial in breast MRI for accurate lesion localization and morphological assessment. It allows radiologists to inspect the shape and position of abnormalities, assess their distance from the nipple, determine their location within the breast, and evaluate potential spread to nearby structures [64].

Modern radiology workstations typically display all three orthogonal planes simultaneously, providing a comprehensive anatomical context for lesion assessment [48]. In addition to these views, often maximum intensity projections (MIPs) are created from the volumetric data [23, 48]. A MIP is a two-dimensional image created by projecting only the brightest (i.e., highest-intensity) voxels along each viewing ray onto a plane. An example of a 3D MIP is depicted in Figure 2.4. While MIPs do not preserve spatial depth, they are

particularly effective for highlighting contrast-enhanced structures such as blood vessels or tumors, which typically exhibit the strongest signal intensities [48].
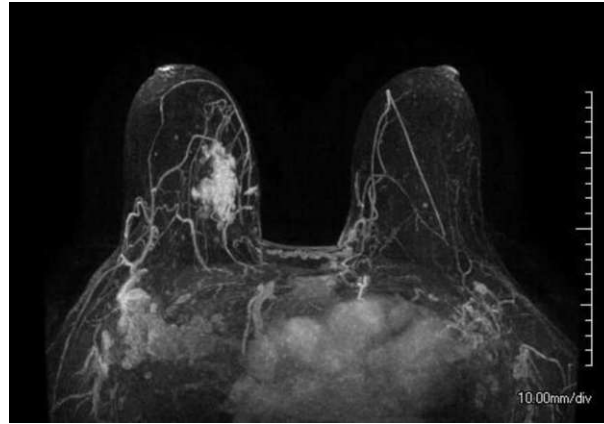

Figure 2.4: Example of a 3D MIP, used to enhance visualization of contrast-enhanced structures such as lesions or lymph nodes (adapted from [60]).

Multiparametric Protocol and Interpretation

A standard breast MRI examination follows a multiparametric protocol that includes multiple sequences, which in combination allow for a comprehensive assessment of breast pathology by evaluating morphology, tissue microstructure, and vascular characteristics [8]. MRI sequences use specific timing patterns of RF pulses and gradient fields to generate images with distinct tissue contrasts. These contrasts are influenced by the interaction between the sequence and the tissue properties, like water content and fat composition [24]. The sequences used for breast MRI inspections are described in more detail in the following:

- **T1-weighted Imaging:** T1-weighted sequences provide high-resolution anatomical images where fat appears bright and fluids appear dark [24]. In dynamic contrast-enhanced (DCE) imaging, contrast agents are administered intravenously. First, a native T1-weighted image is acquired. After contrast material administration, the T1-weighted acquisition is repeated to detect malignancies due to their rapid enhancement pattern [65]. Subtracting these images enhances lesion detection by differentiating truly enhancing structures from lesions with native high intensity. Moreover, a maximum intensity projection (MIPs) from these subtractions can facilitate rapid lesion identification [39].

- **T2-weighted Imaging:** T2-weighted sequences are highly sensitive to water content, making fluid accumulation and cystic structures appear bright [24]. They are useful for differentiating benign from malignant lesions, assessing tissue fibrosis, and identifying architectural distortions, post-therapeutic changes, duct ectasia, and edema [8].

- **Diffusion-Weighted Imaging (DWI):** DWI evaluates the movement of water molecules within tissues, providing insights into the microstructure of the tissue. A key component of DWI is the Apparent Diffusion Coefficient (ADC) map, which is automatically created from diffusion coefficients on a voxel-by-voxel basis [8, 24].

Figure 2.5 provides a representation of a multiparametric breast MRI protocol. Typically, imaging begins with non-contrast acquisitions (T2-weighted and DWI), followed by a native T1-weighted acquisition and then contrast-enhanced series. For breast screenings, the imaging protocol can be abbreviated to precontrast and early postcontrast T1-weighted acquisitions. However, for lesion characterization, incorporating T2-weighted and DWI sequences significantly improves diagnostic accuracy [39].
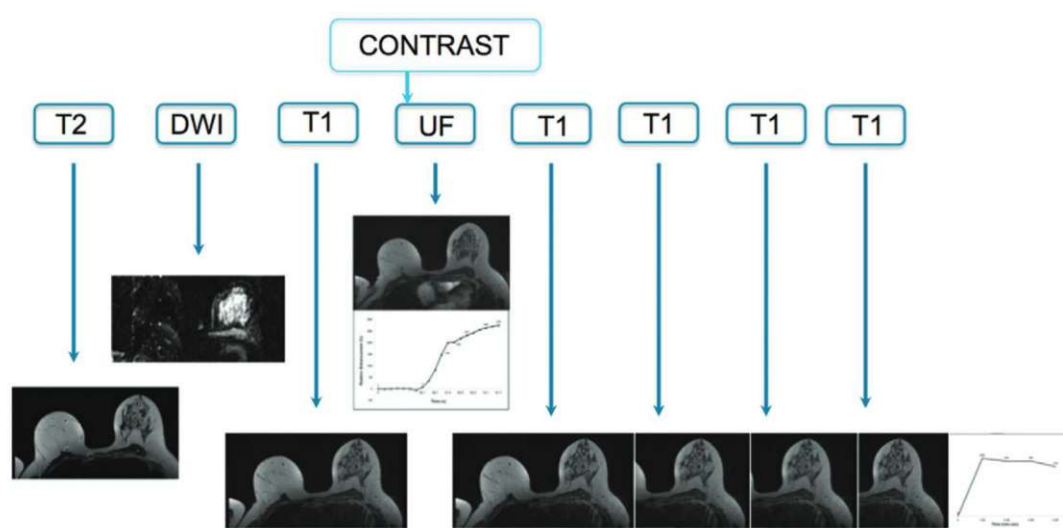

Figure 2.5: Multiparametric breast MRI protocol (from [39]) consisting of non-contrast acquisitions (T2-weighted and DWI), followed by a native T1-weighted acquisition and contrast-enhanced series.

To streamline the breast MRI reading workflow and reduce potential sources of error, standardized hanging protocols are recommended. A digital hanging protocol can define preferred slice orientations, sequence order, and visualization presets, allowing consistency across different cases [48]. Standardized reading layouts help reduce reading time, minimize interpretation errors, and increase diagnostic confidence. Typically, all displayed image series are linked, allowing for simultaneous scrolling and zooming across sequences. Figure 2.6 illustrates an example of a standardized hanging protocol, including multiple sequences such as DWI, T1-weighted, T2-weighted, and contrast-enhanced images with subtractions.

Breast MRI interpretation involves assessing both morphological and kinetic information [19, 39]. Morphologically, enhancing lesions are categorized as foci, masses, or nonmasslike enhancements [19]. Also, lesion size, anatomical location, margin char-
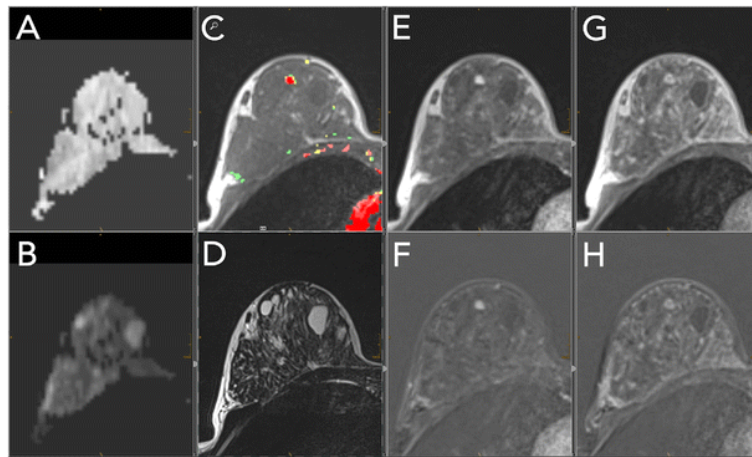
Figure 2.6: Example of standardized hanging protocol for breast MRI (from [16]). The layout consists of ADC map (A), a high b-value DWI image (B), a pre-contrast T1-weighted image (C) and a T2-weighted image (D), followed by early and delayed post-contrast images with corresponding subtractions (E-H) [16].

acteristics, and internal enhancement patterns present morphological descriptors for malignancy [16]. For the kinetic assessment, the time-signal intensity curves (illustrated in Figure 2.7) reflect the contrast uptake over time, revealing important characteristics of the lesion's blood supply [37, 39]. The curve interpretation is divided into two phases: the initial phase describes the speed of enhancement (slow, medium, or rapid), and the delayed phase classifies the enhancement pattern (persistent, plateau, or washout). Lesions that show rapid or medium initial enhancement followed by a plateau or washout pattern have a 77% positive predictive value for malignancy [19, 39].

In order to categorize the kinetic and morphological features described above, standardized systems like the breast imaging reporting and data system (BI-RADS) are used, resulting in a BI-RADS score. However, the BI-RADS lexicon does not directly provide malignancy risk [37, 39]. To address this, the Kaiser-Score combines five diagnostic criteria (such as lesion margins, enhancement patterns, and kinetic curve type) into a decision tree that helps assess the likelihood of malignancy, providing clinical decision rules [16].

Supine Breast MRI

As described above, traditionally, breast MRI is performed with the patient in a prone position. This positioning optimizes image quality by reducing motion artifacts and minimizing interference from the surrounding chest wall [39]. However, prone imaging introduces several challenges. The gravitational deformation of breast tissue causes differences in breast shape and lesion positioning compared to other imaging modalities such as ultrasound [41] or intraoperative views, potentially complicating treatment planning. Prone positioning can also be uncomfortable [31], and the lack of physical support for the hanging breasts may increase motion artifacts [14]. Another limitation is
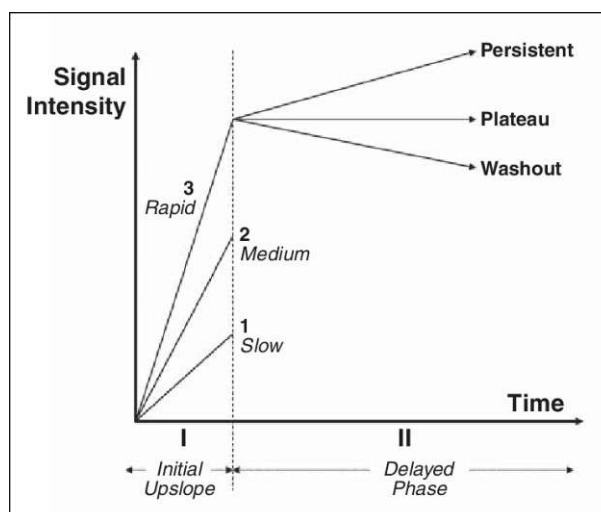
Figure 2.7: Time–signal intensity curves for kinetic assessment in breast MRI (from [19]). The curves illustrate initial uptake (slow, medium, or rapid) and delayed enhancement patterns (persistent, plateau, or washout), aiding in lesion characterization.

the design of the RF coils, which have to be optimized for rather large breasts in order to allow them to fit into the coil openings. This results in a lower signal-to-noise ratio in patients with smaller breasts, but also restricts applicability for very large breasts that do not fit into the coil.

Supine breast MRI offers an alternative that addresses many of these limitations by better aligning with other clinical workflows. Obermann et al. [43] introduced a wearable RF coil vest ("BraCoil", illustrated in Figure 2.8), enabling MRI acquisition in a supine position.

Figure 2.8: Supine MRI acquisition using the BraCoil (adapted from [43])

The supine position is generally more comfortable for patients [42]. Since ultrasound-guided biopsies and surgeries are also performed in this orientation, supine imaging improves spatial correlation, enhances lesion localization, and facilitates second-look ultrasound evaluations [41]. This alignment can reduce the need for MRI-guided biopsies, which are more time-consuming and costly.

Despite their advantages, supine MR images also present new challenges. The breast is less extended in this position compared to prone imaging, which can make it more difficult to precisely localize lesions and assess their relation to anatomical structures such as the nipple. Figure 2.9 depicts a direct comparison of a MRI image acquired in the prone (A) and supine position (B), illustrating the tissue spread. This demonstrates the need for a new visualization approach that enables a more comprehensive view of the breast volume within fewer slices.
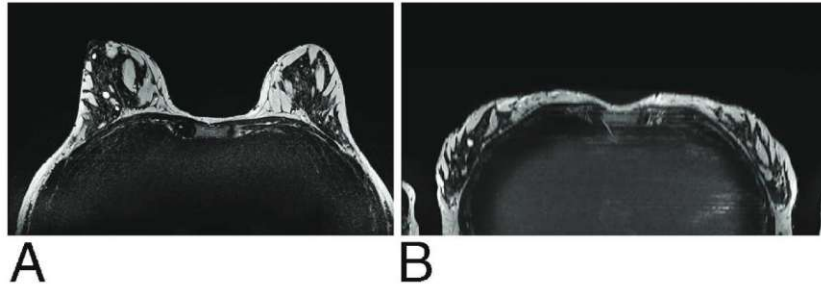
Figure 2.9: Comparison of breast tissue distribution in prone (A) vs. supine MR images (B) in the axial plane (adapted from [43]).

2.4   MRI Dataset Employed in this Thesis

The dataset used in this thesis consists of MRI scans acquired in the supine position using the BraCoil system [43]. It includes imaging data from three healthy subjects with different breast sizes — small ($\approx$ 600 ml), medium ($\approx$ 1300 ml), and large ($\approx$ 3000 ml). For each healthy subject, the dataset contains both T1-weighted and T2-weighted sequences without contrast agent. In addition to the healthy subject data, the dataset also includes a scan from a patient volunteer with pathological findings, containing T1-weighted scans with and without contrast agent, T2-weighted images, as well as diffusion-weighted images ($b = 0$ s/mm^2 and $b = 800$ s/mm^2) with reconstructed apparent diffusion coefficient maps. Subjects were measured after written informed consent within a study approved by the Local Ethics Committee (EK Nr. 2137/2021).

CHAPTER 3

Related Work

As a first step for this work, a thorough literature analysis was carried out. The search was conducted by using keywords such as "flattening techniques", "medical imaging" and "breast MRI visualization". Search engines like Google Scholar, IEEE Xplore, Springer and ScienceDirect were used. The main focus was on recent publications, starting from 2018. However, earlier publications were also included for a general understanding of MRI procedures and visual computing techniques. The inclusion criteria were based on relevance to breast MRI visualization and volumetric image flattening techniques in medical imaging. Following the literature research, the identified techniques were analyzed and compared, with focus on the different methods carried out to flatten medical images.

Table 3.1 represents a summary of the reviewed paper in terms of reformation technique, input and output of the reformation and on which medical entity the paper focused. As only one study was found that specifically addressed flattened visualization of breast MRI [43], additional papers were included that applied similar flattening techniques to other medical entitites. Based on the reformations, three broad categories were identified: Curved Planar Reformation (CPR), surface-driven reformation and continuous volumetric parameterization.

3.1 Curved Planar Reformation

CPR is one of the most well-known examples of anatomical reformation techniques [49] and commonly employed in order to assess tubular structures, like blood vessels, bronchi, and the colon. By using the object's central axis the structure can be made visible within one image in its entire length. The central axis's position and shape determine which parts of the 3D space are visualized. To improve visualization, a vector of interest is added, as the surface is not well defined by just one curve. This vector together with a point on the central axis, define a line of interest. All voxels along this line are used to

Table 3.1: Reviewed literature structured by employed reformation technique.

Reformation Technique	Medical Entity	Input	Output	Source
CPR	Tubular Structures	Centerline	2D Visualization	[30]
CPR	Brain	Centerline	2D Visualization	[58]
CPR	Breast	Centerline	Volumetric Mesh	[43]
Surface-driven	Bone Structures	Surface Mesh	Volumetric Mesh	[34]
Surface-driven	Placenta	Surface Mesh	Volumetric Mesh and standard 2D Map	[40]
Volumetric Parameterization	Placenta	Tetrahedral Mesh	Volumetric Mesh	[6]

re-sample the volume. There are three different forms of CPR: projected, stretched, and straightened (see Figure 3.1), from which straightened is preferred for many applications. Straightened means, that the height of the resulting image is equal to the length of the central axis. In Figure 3.1, the horizontal plane represents the image, with the image's y-axis shown as a horizontal blue arrow. The curve in the 3D data set is indicated by the vertical blue arrow [30].
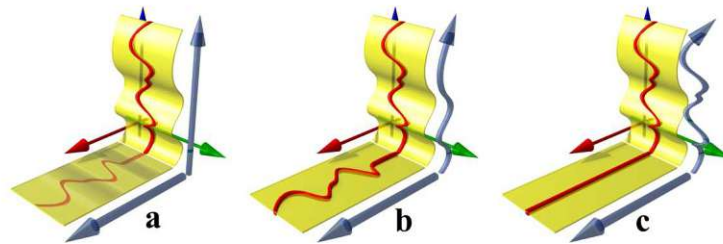
Figure 3.1: CPR generation methods: a) projected, b) stretched and c) straightened (from [30]).

One limitation shared by all three forms of CPR is that their accuracy depends heavily on the quality of the extracted centerline. Additionally, only the parts of the vessel that intersect the resampled plane are visualized. To address these issues, Kanitsar et al. [30] proposed Thick-CPR, which includes not only the centerline plane but also a surrounding volume within a predefined thickness. This extended subvolume is visualized using reformatting techniques such as voxel averaging or MIP, again resulting in a 2D representation.

Simpson et al. [58] apply CPR in order to analyze characteristic brain surface changes of children, who experienced a brain damage as newborns. They highlight that the resulting flat-earth maps could be of help when communicating with clinicians and non-medical

specialists, like legal professionals and parents. This technique involves manually setting curves to ensure the most relevant brain regions are visualized (see Figure 3.2, left). To flatten the brain image, they place two curves: one at the coronal plane and one at the sagittal plane, at slices which provide the best overview of the cortical regions most frequently damaged by the particular brain injury. They create two types of flattened maps from these curves: a mercator map and a scroll map. A mercator map, similar to the classical mercator projection used for mapping the earth, represents the 3D surface of the brain on a 2D plane, preserving angles but distorting size, particularly towards the edges (see Figure 3.2, right a). In contrast, a scroll map unrolls the brain surface into a continuous strip, providing a linear view of the brain's structures (see Figure 3.2, right b). The authors note that while there are automated methods for creating CPR on the brain surface, these often require expensive, specialized software. In contrast, for their manual approach they use software bundled with commercially available MRI scanners.
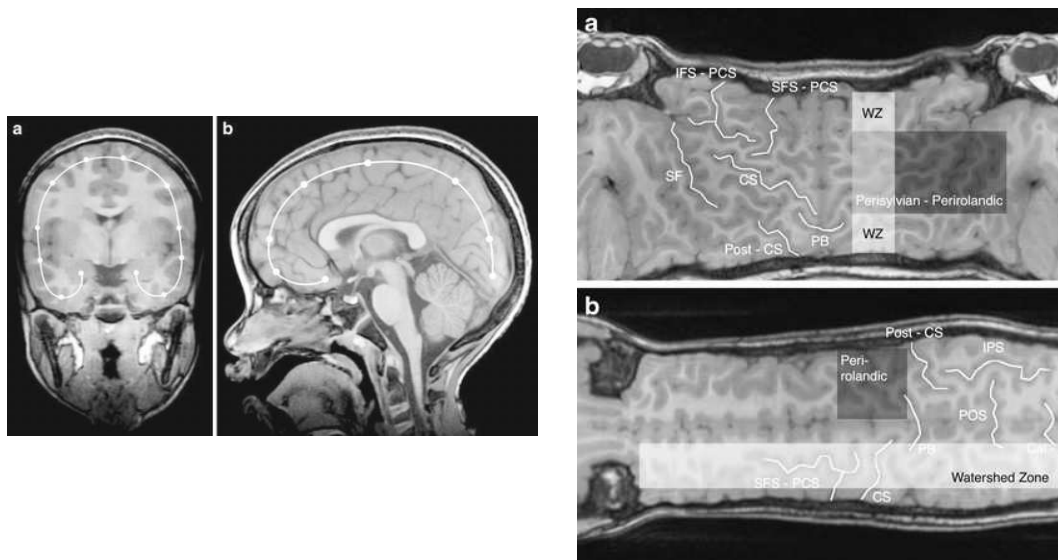
Figure 3.2: Curved planar reformation (CPR) for brain surface analysis (from [58]). Left: landmark placement. Right: resulting mercator projection (a) and scroll map (b).

Next to straightening of tubular structures and brain images, CPR was also applied for breast MRI visualizations. For the supine breast MRI, described in Section 2.3.3, Obermann et al. [43] introduce a panoramic visualization in order to reduce the number of slices containing breast tissue, which consequently reduces the effort for radiologists. The visualization was created by two consecutive CPRs, one performed along the sternum and the second along the breast shape. Here again, the curves for the reformation were placed manually (see Figure 3.3, orange and blue curves). The authors highlight, that the second line for the reformation (blue curve) should be drawn through the breast tissue with equal distance between body surface and chest wall, in order to minimize geometric distortions.
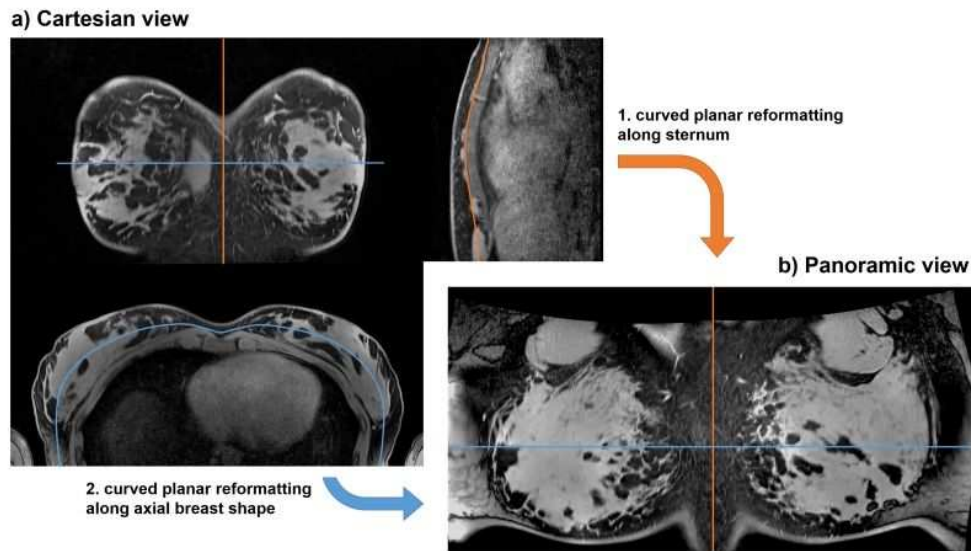
Figure 3.3: Panoramic breast MRI using two consecutive CPRs with manually placed reformation curves in blue and orange (from [43]).

For this panoramic breast MRI, the authors employ an implementation [4] of the Straightened CPR method originally described by Kanitsar et al. [30]. However, unlike the Straightened approach described above, their method retains the full volume information. Instead of flattening the sampled data into a single image, the surrounding volume slab is resampled and straightened according to the centerline, resulting in a flat but volumetric representation of the anatomy. Figure 3.4 shows the volume slab following the centerline in yellow, where the slice size determines the thickness of the resulting volume.
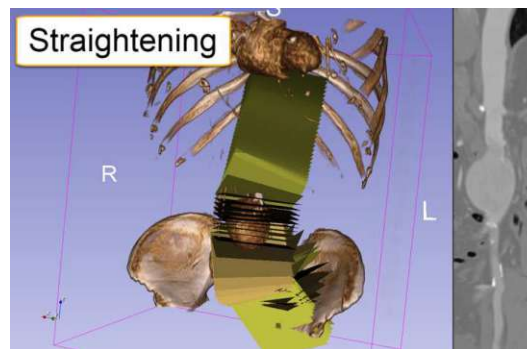
Figure 3.4: Volumetric CPR in 3D Slicer: a slab volume is resampled and straightened along a centerline (yellow) resulting in a 3D image (adapted from [4]).

The authors note that the panoramic view could reduce the number of slices to be reviewed by a factor of 2–4 compared to the standard view. An example is illustrated in

Figure 3.5, showing a 3D rendering of segmented breast tissue (top row) alongside the corresponding T2-weighted images (center row).

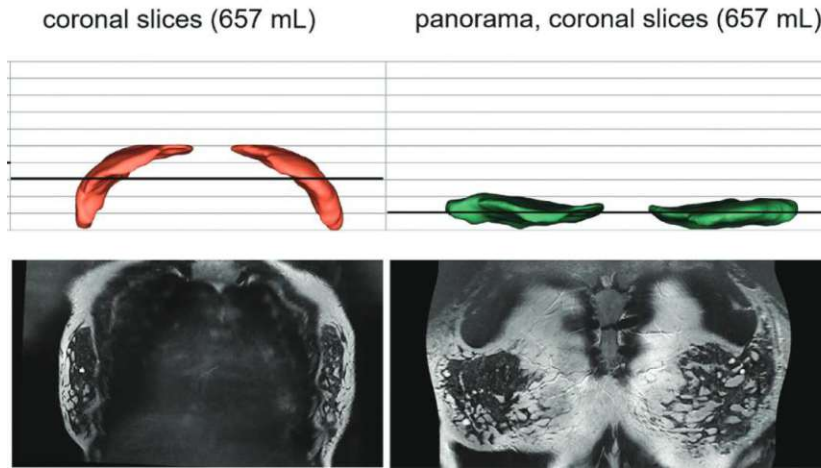coronal slices (657 mL)   panorama, coronal slices (657 mL)

Figure 3.5: Panoramic breast MRI (right) compared to the standard coronal view (left), demonstrating a reduction in the number of slices required for interpretation (adapted from [43]).

3.2 Surface-driven Reformation

Kretschmer et al. [34] introduce anatomy-driven reformation (ADR), which they describe as generalization of Multiplanar Reformation (MPR) to curved surfaces. MPR is a technique, which allows for a more flexible inspection through reorienting the original medical dataset. Anatomy-driven refers to the fact that the medical volumes are reformatted based on the individual anatomical geometry of a patient. The input for ADR represent triangular surface meshes, which is placed in the center of the anatomical structure. Based on this, a non-linear and as-rigid-as-possible (ARAP) volumetric deformation is applied. As in MPR, reformations are based on surfaces, where they employ the ARAP approach defined in the study of Lui et al. [35]. However, to parameterize the surrounding area of the ADR surface, they borrow from the field of volumetric deformation. In order to include this surrounding area and allow for slicing, the authors parameterize not only the surface but also its offset surfaces. They highlight that the approach can be applied to various anatomical entities and demonstrate reformation examples of different bone structures (see Figure 3.6).

To arrive at the reformation, as first step offset surfaces are computed from the initial ADR surface (see Figure 3.7, step 1), using the vertices' normal vectors. Here copies of the surface mesh are created with negative and positive displacements, resulting in three layers. Consequently, the surface mesh and its offset layers are flattened (step 2). This involves deforming the meshes into flat layers, while minimizing intra-layer distortions to preserve the anatomical geometry as much as possible. Finally, the flat volume is created
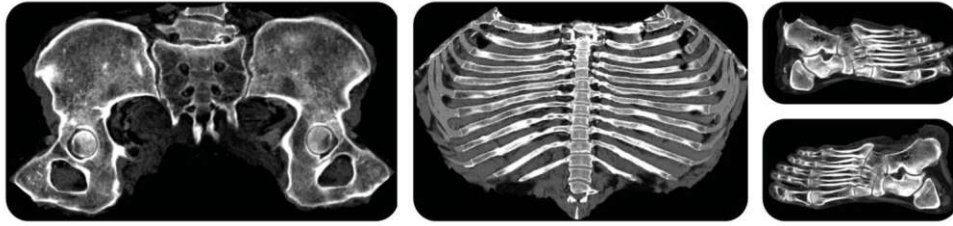
Figure 3.6: ADR applied to different anatomical structures: pelvis, rib cage, and feet (from [34]).

by resampling the original 3D dataset based on the flattened mesh layers (step 3). For the initial flattening, they use a harmonic triangulation by Floater [21], which is then refining using the ARAP approach [35].
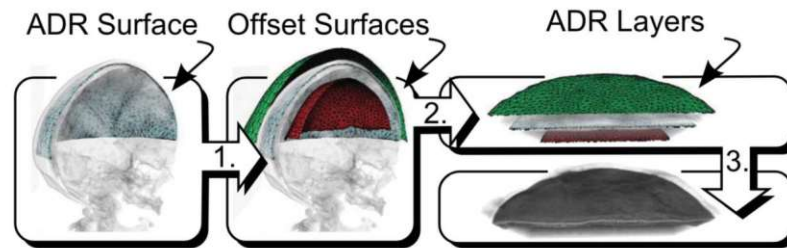

Figure 3.7: Steps of ADR process (from [34]). (1) Computation of offset surfaces from the initial anatomical surface (2) Flattening of the original and offset meshes (3) Resampling of the original 3D volume.

Similarly to the ADR approach, Miao et al. [40] create a flattened visualization for clinicians to analyze reconstructed images by scrolling through different slices. This work focuses on the flattened visualization of the placenta, mimicking its physical ex vivo (post-birth) shape, which is predominantly disk-like, flat, and round. The authors identified four steps for the deformation: First, the placenta is automatically motion-compensated and segmented. Secondly, from this segmentation, a Euclidean distance field and iso-surfaces are created to compute offset surfaces at 1mm intervals. As third step, the fetal and maternal sides of the placenta are automatically identified and separated (see Figure 3.8, top row). Each part is flattened separately by using the mean value coordinates approach, which maps the boundary points of the placenta surface to a disk. Interior points are projected inside the disk using convex combination mapping, ensuring minimal distortion by maintaining the relative positions of points. They employ the mean value coordinates approach of Floater [22] for this parameterization. Finally, a standardized 2D map view is created (see Figure 3.8, bottom row), allowing for comparison of multiple placentas.
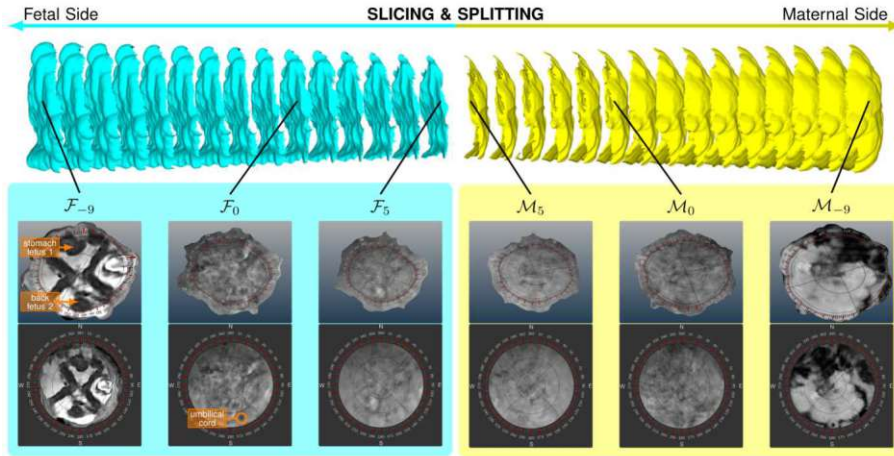
Figure 3.8: Placenta map (from [40]) illustrating sliced placenta layers (top row), flattened MRI views (middle row) and standardized 2D placenta maps (bottom row).

3.3 Continuous Volumetric Parameterization

According to Abulnaga et al. [6], due to the independent parameterization of the 2D surface in each slice, there is no alignment across layers when using the approach proposed in the work of Miao et al. [40]. This can lead to distortion of important depth image information. Thus, Abulnaga et al. [6] propose a continuous volumetric parameterization for placenta flattening without a fixed boundary. First, the placental shape is modeled as tetrahedral mesh, which can be extracted from a placenta segmentation of a MRI scan. The mapping is then parameterized by using the mesh vertex locations. The deformation is interpolated to the interior of each tetrahedron by applying a locally affine model. They evaluate three different templates, one with two parallel planes for the thickness (a), one with an ellipsoid for the shape of the unfolded placenta (b) and a single plane (c), which represents a relaxation of the parallel planes (see Figure 3.9).
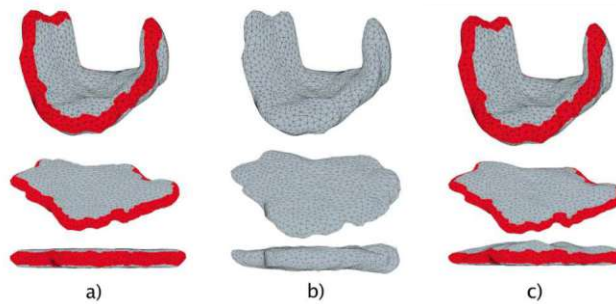

Figure 3.9: Volumetric parameterization showing the original (top row) and flattened meshes (bottom row) using different templates: a) parallel planes, b) ellipsoid, and c) single plane (adapted from [6].

21

The authors recommend the parallel planes template for most use cases, as this results in a parameterization with less distortion compared to the ellipsoid and is more natural for visualization with 2D cutting planes. The comparison between the MRI slices mapped from the flattened volume and cross-sections of the original volume are illustrated in Figure 3.10.
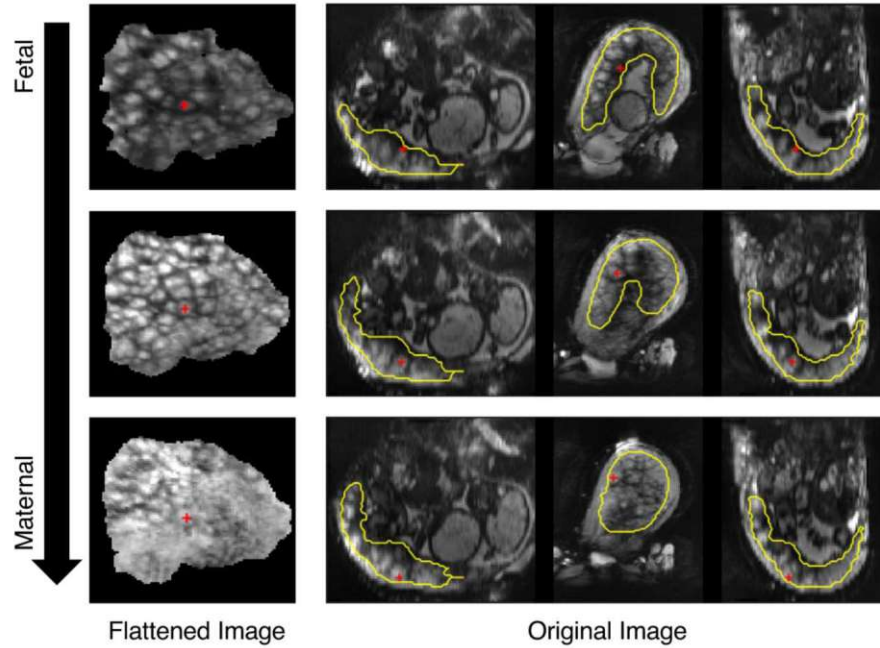

Figure 3.10: Comparison of MRI slices from the flattened placenta volume (left) with corresponding cross-sections from the original volume (right) using the parallel planes template (from [6])

3.4   Summarization

CPR requires a centerline to straighten the surrounding volume, allowing for more flexible inspection of tubular structures such as blood vessels, bronchi, or the colon. However, CPR has limitations, including the need for manual placement of reformation curves [43, 58]. Automated methods are needed to ensure more consistent and reliable results across different cases. Another significant limitation is CPR's generation of only 2D visualizations rather than scrollable 3D volumes. This constraint can lead to loss of important depth information, particularly in applications like breast MRI. Although Obermann et al. [43] employ CPR to achieve volumetric outputs, their work currently relies on just two lines, which does not represent the complex shape of the breast. This simplification leads to higher distortions, particularly noticeable at the edges and corners of the image. Additionally, a major challenge with this approach is the risk of self-intersections in the displacement field (see Figure 3.11). When the slice size is too large

or the curve resolution too fine, the transformation may map the same source point to multiple target positions, causing the displacement field to fold [4].
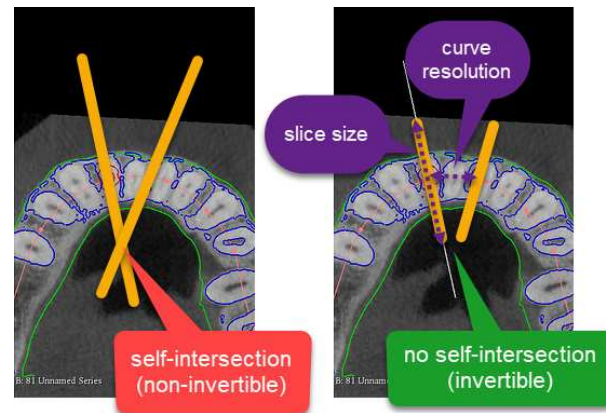

Figure 3.11: Self-intersection issues in CPR. Left: overlapping slices producing self-intersections. Right: properly set slice size and curve resolution (from [4]).

Surface-driven approaches, utilizing surface meshes, offer a solution to the simplification limitations observed in CPR, as discussed in [43]. These methods have shown potential to achieve more accurate volumetric reconstructions [34, 40]. However, as noted by Kretschmer et al. [34], the use of offset surfaces can also introduce self-intersections, potentially complicating the accuracy of the reconstructed volumes. In order to address this issue, Miao et al. [40] employ distance fields instead of normal vectors to calculate the offset surfaces. This ensures that there are no self-intersections and should establish a well-defined surface. Another limitation with surface-driven reformation techniques is their sensitivity to the precision of the input surface data. Variations or inaccuracies in the initial surface representation can directly impact the quality of the reconstructed volume. Moreover, these methods also lack in alignment across layers of the anatomical structure. The discrete slicing approach used in the listed surface-driven methods can lead to distortions and information loss between layers, which may limit the understanding of the anatomical details. This limitation is addressed by continuous volumetric parameterization, which takes a tetrahedral mesh as starting point. According to Abulnaga et al. [6] this approach ensures consistency and minimal distortion. However, their parameterization relies on templates like flat planes or ellipsoids, which it is not suitable for the complex geometry of breast MRI.

In summary, each existing flattening technique offers specific advantages and forms the foundation for our work. However, only limited efforts have been applied to breast MRI, particularly in the supine position, and the existing approach does not fully resolve its complex geometric challenges. This gap motivates our investigation into whether flattening-based visualization methods can enhance the interpretability and clinical utility of supine breast MRI.

CHAPTER 4

User Requirements

Following a human-centered approach we conducted user- and expert interviews to gain deeper insights into the requirements for the new visualization. This approach allowed us to better understand the specific needs and preferences of the intended users, as well as the expertise and technical challenges identified by professionals working in the field of breast imaging.

4.1   Interview Methodology

A semi-structured qualitative study from the field of human-computer interaction was carried out, inspired by the work of Blandford [10]. Specifically, a semi-structured interview was used, which is an approach that combines predefined questions with the flexibility to explore emerging topics. This involved in-depth interviews with radiologists and visualization experts to gather insights into their workflows, challenges, and expectations. The interviews were conducted using a semi-structured interview guide to provide structure, yet flexibility. The complete interview guide can be found in the appendix (see Appendices A and B).

4.1.1   Recruitment and Participants

We recruited four participants for our interviews through the Medical University of Vienna. Two of the interviewees were radiologists with more than 10 years experience in the field of breast MRIs, and will be referred to as "users" in the following. The remaining two participants were medical physics experts specializing in magnetic resonance imaging, with more than five years of experience working on flexible coils for supine breast MRI. These participants will be referred to as "experts" in the subsequent analysis. The experts also played a key role in creating our current baseline visualization [43], which served as a foundation for the design of new visualization methods.

4.1.2   Data Collection

The questions asked in the interview were designed to gain insights into the radiologists' diagnostic workflow, the challenges they face, and their needs in lesion detection and diagnosis. Key aspects, like the most important regions of the breast that require focused visualization, specific landmarks or reference points essential for diagnosis were clarified (see Appendix B). Additionally, medical physics experts were asked to share insights into the special challenges of supine breast imaging, particularly in comparison to the prevalent visualizations in prone position (see Appendix A). Both participant groups were also shown initial ideas of possible deformation processes in the form of axial breast images with grid-overlays and asked which mock-up version they preferred. Our data consisted of the audio-recorded interviews and handwritten notes by the author of this thesis.

4.1.3   Procedure

The interviews took place at the Allgemeines Krankenhaus der Stadt Wien (AKH, General Hospital of the City of Vienna), at the interviewees' workplaces. All interviews were conducted in German and lasted approximately 40 minutes to one hour. Before the interviews, all participants signed an informed consent form, which also included a data protection agreement.

The audio files of the interviews were partly transcribed manually and combined with the handwritten notes by the interviewer. All identifying information was removed prior starting the analysis. For the analysis of our qualitative data, we followed the thematic analysis approach described by Braun and Clarke [12], chosen for its flexibility. A thematic analysis is a method for identifying, analyzing, and reporting patterns within qualitative data. An inductive approach was used, allowing codes and themes to emerge directly from the interview data. The author of the thesis manually reviewed the transcripts and notes, coded them, iteratively grouped related codes into broader themes and refined them across multiple readings.

4.2   Thematic Analysis

In the following the emerging themes and sub-themes of the thematic analysis are described to give a better understanding of the patterns across the results of the interviews. Figure 4.1 depicts an overview of the identified themes, sub-themes and codes. Direct citations were translated from German.

Deformation Mock-up

In the course of the interviews the participants were shown conceptual representation of different deformation possibilities (see Figure 4.2). We introduced a set of preliminary designs, created in collaboration with my supervisors and inspired by the state of the art, as a foundation for iteration and further refinement. These mock-ups explored three key
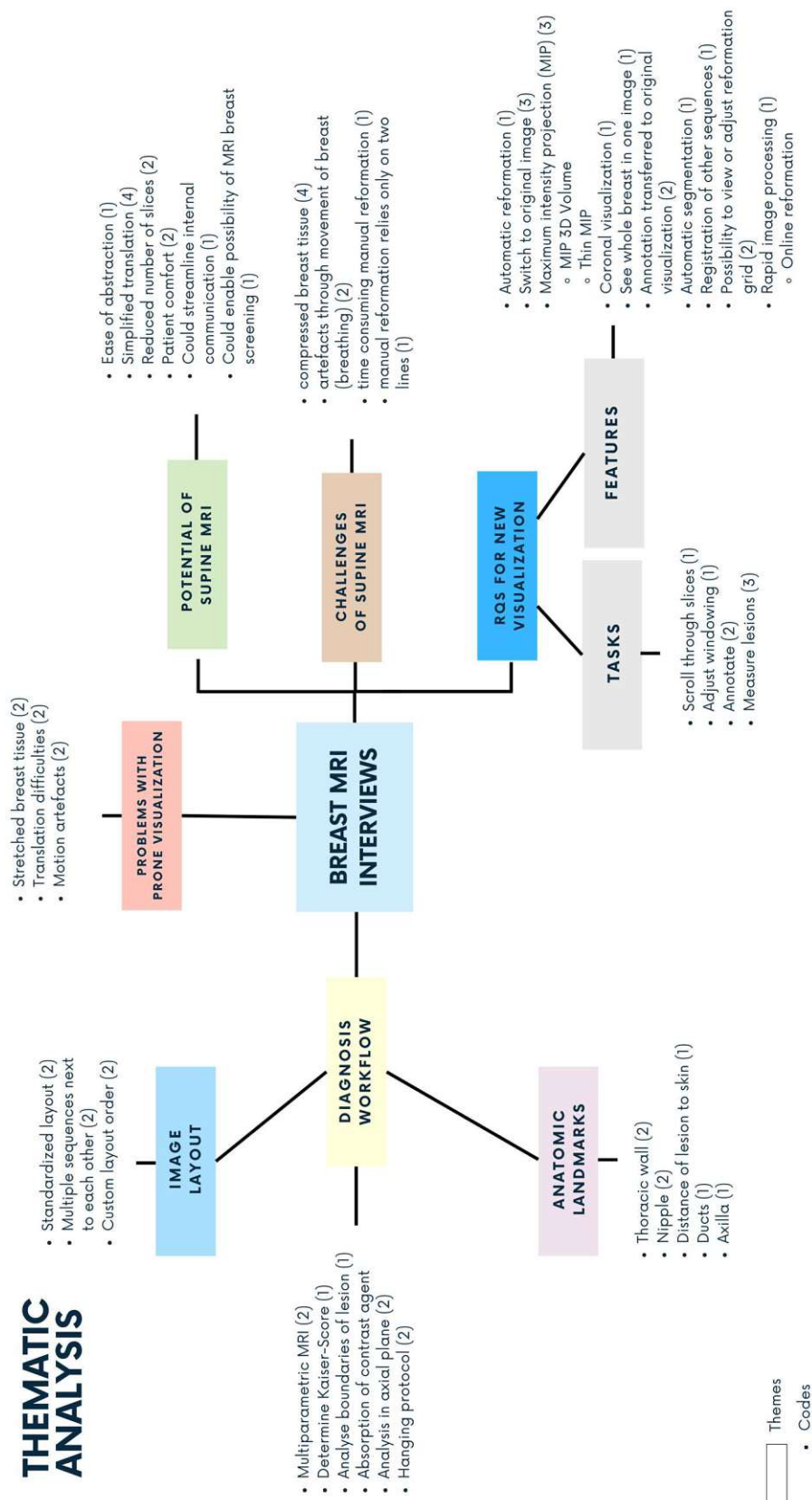
Figure 4.1: Thematic analysis of user and expert interviews, showing the identified themes, sub-themes, and associated codes derived from qualitative analysis. The number of occurrences is indicated in parentheses.

directions: deforming the breast based on the surface (Version 1), applying a uniform grid structure based on the rib cage (Version 2), and deforming the breasts independently (Version 3). The deformation grid is highlighted by the orange lines in each version. Three out of the four participants preferred version 2 of the mockup, while the fourth participant stated that they would need to see an example before determining which version is better. The majority found version 2 clearer and less repetitive, suggesting that it could help radiologists better interpret the images, as one participant explained: "I would tend to choose version 2 simply because otherwise you see the same thing 100 times and that could be confusing." Another participant noted: "I think maybe radiologists can imagine it better this way, because if the gap is visible in the middle, they know where they are in the image." A third version, in which the breasts were displayed separately, was also shown. However, all participants agreed that it is essential to view both breasts simultaneously and therefore did not consider this version suitable.
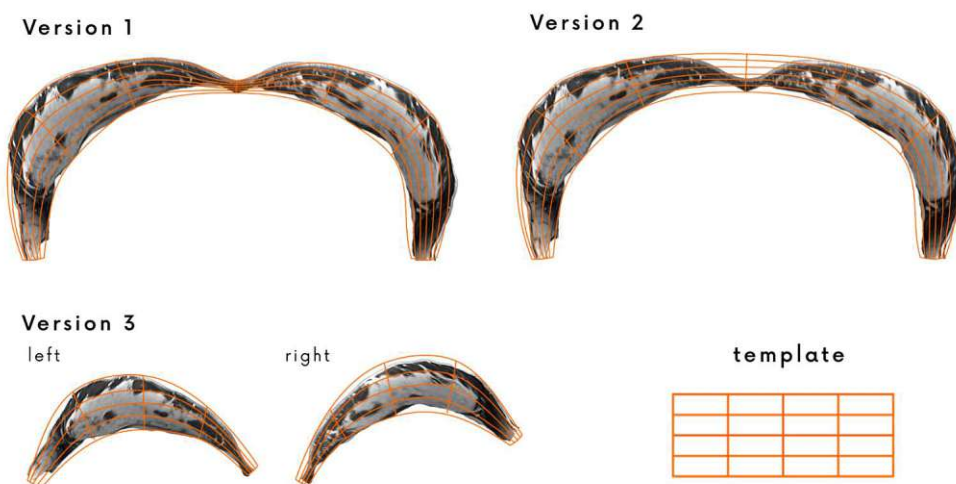
Figure 4.2: Mock-ups of different deformation strategies: 1) deform along surface, 2) use a uniform grid, 3) focus on breasts separately.

4.2.1 Diagnostic Workflow

One emerging theme (see Figure 4.1) focused on the radiologists' diagnostic workflow in breast MRI procedures. A central finding was the heavy reliance on axial visualization of the breast during MRI. Radiologists consistently emphasized that, due to the prone position of the patient, the breast tissue is stretched, making enhancements most visible in the axial plane. This orientation is preferred because it offers optimal visibility of the breast tissue, allowing for more accurate detection of abnormalities.

Radiologists emphasized the morphological analysis and the importance of closely analyzing the boundaries of a lesion. The shape is particularly important when it is either irregular or well-circumscribed, as these characteristics can suggest different levels of malignancy.

Additionally, the use of a multiparametric MRI was identified as a central component of the diagnostic workflow. As described in Section 2.3.3, this technique combines multiple imaging sequences to provide a comprehensive assessment of breast tissue. Both radiologists described that the absorption of contrast agents plays a significant role in lesion detection and characterization. The visual assessment of how a lesion absorbs the contrast agent can indicate its nature, helping to distinguish between benign and malignant lesions. One interviewee also described using the Kaiser-Score [16] as part of this process.

Hanging Protocol

A related theme that emerged during the interviews was the use of a grid-based layout (see Figure 4.1), known as a hanging protocol, to view multiple sequences simultaneously. These consist of the T1 original image, T2 weighted sequence, diffusion-weighted images, ADC (Apparent Diffusion Coefficient) map, peak enhancement, and late enhancement. An example figure of such a hanging protocol can be found in Section 2.3.3. Both radiologists emphasized the importance of a customizable layout, noting that it is crucial for the order of images to be consistent and to open in the same standard setup for each patient.

Anatomical Landmarks

Radiologists pointed out specific areas or landmarks that are particularly relevant during the inspection. The thoracic wall was mentioned as an important area, especially in the context of ultrasound inspections or surgical planning. The nipple serves as an important landmark for determining the location of a tumor, particularly in relation to the surrounding breast tissue. In surgical contexts, the tumor's distance to the skin is also a significant consideration. Additionally, the axilla and its lymph nodes were described as important regions for diagnosis, particularly in assessing the spread of malignancy.

4.2.2 Problems with Prone Visualization

In order to gain a deeper understanding, participants were asked for the current challenges and problems with the prone visualization (see Figure 4.1). A major challenge, highlighted by one radiologist and one medical physics expert, is the difficulty in translating findings from the prone MRI to procedures, such as biopsies, which are typically conducted in the supine position. The displacement of breast tissue between these positions can make it challenging to accurately locate a lesion identified on the prone MRI during a subsequent biopsy [41]. One participant described that if the lesion cannot be found using ultrasound-guided biopsy (which is less invasive and more comfortable for the patient), an MRI-guided biopsy may be required. This procedure is not only more expensive but also more uncomfortable for the patient.

Another significant issue raised by two interviewees is that the breast tissue is stretched due to gravity when the patient is in prone position. The design of the RF coils presents

another limitation, as it restricts applicability for very large breasts. As one participant explained: *"In the standard prone position, the breast hangs into two openings and the tissue is stretched and pulled away from the chest wall [..] but the problem is, if the breast is too large for the coil, folds can form or the breast is pressed into an odd shape"*. On the other hand side, since the coils are often designed for larger breasts, smaller breasts may not be adequately supported or stabilized within the coil. This can lead to increased movement during the scan, resulting in motion artifacts that degrade image quality [14]. To mitigate these artifacts, radiologists and technologists sometimes use paper towels or foam to fill the space and stabilize the breast, which again can cause discomfort for the patient.

4.2.3 Potential of Supine MRI

The interviews highlighted several advantages of using a supine position during breast MRI, particularly in terms of clinical application and workflow efficiency. All four participants highlighted the simplified translation as one major benefit of the supine position. Particularly its ability to simplify the translation of MRI findings to other clinical procedures, such as biopsies, surgeries, and radiation therapy was noted. One radiologist emphasized this point, noting: *"This [the coronal plane] is what I see in the clinic, both for the surgeon and for me when I perform a biopsy [...] That's the innovation potential of the Bracoil: that I don't have to spend much time thinking about it. Because for many, abstracting from this [axial] to ultrasound is nearly impossible."*

Another advantage discussed was the potential to simplify the imaging process. By using techniques like MIPs or Thin-MIPs, the number of images that need to be reviewed could be significantly reduced, easing the workload on radiologists. This reduction in number of slices could make the reading-process less time-consuming and resource-intensive. One medical physics expert emphasized that this simplification could enhance the overall efficiency of breast radiology departments.

Patient comfort was mentioned by both medical physics experts as a notable benefit of the supine position. While a few patients expressed comfort with the prone position, the majority found the supine position more comfortable. One expert explained that the supine position also holds promise for future breast screening tools. With advancements in coil technology and the potential for faster imaging, the supine position could be integrated into routine screening, making the process quicker and more effective. Additionally, one radiologists and one medical physic expert noted that a new visualization could improve communication and standardization between clinicians, potentially leading to more streamlined and effective treatment planning.

4.2.4 Challenges of Supine MRI

While the supine position in MRI offers several benefits, the interview participants identified a number of challenges. A prominent issue raised by all four participants is the compression of breast tissue in the supine position. When patients lie on their

backs, gravity causes the breast tissue to flatten and spread across the chest wall. This compression can make it difficult to visualize lesions clearly, as one radiologist noted: *"I think interpretation becomes more difficult because we likely can't evaluate the lesion's margin as well, simply because the tissue is more compressed. When the patient is in prone position, the breasts are nicely distributed, giving us much more space to assess small lesions."*

Another significant challenge discussed by the experts is the increased likelihood of motion artifacts in the supine position. As the breast moves with the patient's breathing, the images can become blurred, especially if the patient is nervous or anxious, which is common in clinical settings where biopsies or surgeries are upcoming.

Additionally, the complexity of current panoramic visualization techniques was highlighted as a challenge by the experts. One participant noted: *"The manual setup is simply time-consuming, and often it fails because the computer's processing power isn't sufficient, it takes 10 minutes just to generate the panoramic visualization."*

Finally, the limited visualization in axial slices when using the supine position was also mentioned. Because the breast tissue is more compressed and spread out, the axial view often provides only a thin strip of tissue to examine, which can make it harder to assess the full extent of the breast tissue. This limitation necessitates the use of alternative views, such as coronal imaging, to ensure that critical areas are adequately visualized.

4.2.5 Requirements for New Visualization

Participants were asked about the required spacing between image slices. For T1-weighted breast MRI, a slice thickness of no more than 2.5 mm is typically recommended to ensure sufficient anatomical detail. Morphological evaluation requires even finer resolution, with an in-plane pixel size of 1 mm or smaller to accurately assess tissue structures [39]. The radiologists indicated that a general maximum slice thickness of around 2 mm would be appropriate. An expert further specified that for supine MRI acquisitions, the in-plane resolution is approximately 0.6 mm, with a slice thickness of about 1.5 mm in the anterior-posterior direction, which should be maintained.

Additionally, the interviewees were encouraged to describe their "ideal" visualization and the features or tasks they would like to perform within it beyond the mock-ups we showed them. In the context of the interviews, the concept of a new visualization refers to improved methods for viewing and interacting with supine breast MRIs. This includes enhancements in how images are displayed (e.g., through specific hanging protocols), as well as how they can be navigated and how reformatted, flattened images can be compared to the original breast images. The following features and tasks emerged from their responses. In this context, tasks refer to the specific actions that users want to perform using the system, features describe the functionalities of the prototypes that enable these tasks.

Tasks

- **Scroll Through Slices**: The system shall allow users to scroll through image slices easily to examine different layers of breast tissue.

- **Adjust Windowing**: The system shall provide the functionality to adjust windowing (brightness and contrast) to enhance visibility and improve diagnostic accuracy.

- **Annotate**: The system should enable users to annotate images in order to mark important areas or findings. This aids in documentation and communication, ensuring that critical information is clearly noted.

- **Measure Lesions**: The visualization tools should support correct measurement of lesions in both the flattened and standard views for diagnosis and surgical planning.

Features

- **Automatic Reformation**: Participants emphasized the necessity for an automated image reformation. One radiologist noted that manual adjustments are impractical, as radiologists' primary focus should remain on image interpretation. Automated reformation processes would streamline workflows and reduce manual intervention.

- **Switch to Original Image**: A frequently mentioned theme was that users require the ability to easily switch between panoramic and standard views, or to display them side-by-side. One radiologist stressed that in order to get used to a new visualization, it is crucial for them and for other departments to see the original axial view they are currently used to.

- **MIP (Maximum Intensity Projection)**: The possibility to create a MIP was mentioned by one radiologist and both experts. Both a thin MIP and the creation of a MIP 3D volume were considered highly beneficial for analyzing the visualization.

- **Coronal Visualization**: The interviewees noted that the coronal view would be best for visualizing supine images. This alignment with the positions used in biopsies and surgeries simplifies the process of locating and correlating lesions across different imaging modalities.

- **Whole Breast in One Image**: One radiologist mentioned that the ability to view the entire breast in a single image or with minimal slices is crucial. This comprehensive approach helps in avoiding missed areas and provides a complete overview of the breast tissue.

- **Annotations Transferred to Original Image**: Annotations made in one view, e.g., the flattened image, should be transferable to other views. This ensures that regions of interest are consistently marked and tracked across different imaging perspectives.

- **Segmentation**: One expert mentioned that segmentation of breast tissue from surrounding anatomical structures, such as the chest wall and ribs, is necessary. This prevents interference from non-breast tissues in MIP views and enhances the clarity of the breast tissue.

- **Registration of Sequences**: As highlighted by one interviewee, synchronization and registration of multiple imaging sequences (e.g., T1, T2, diffusion) are crucial. This ensures accurate interpretation and comparison across different imaging modalities.

- **Possibility to View Reformation Grid**: Displaying a grid over reformed images may assist radiologists in understanding the spatial relationships and orientation of slices, improving navigation and assessment. One interviewee mentioned that they would also like to have the possibility to correct the reformation grid if necessary.

- **Rapid Image Processing**: Efficient processing of imaging data is vital for handling high volumes of cases. The system must be capable of rapid image processing to meet the demands of radiologists who need to review and report on multiple cases quickly. One radiologist mentioned that they perform around 50 diagnoses per day, so they need to be able to complete 10 diagnoses per hour with the visualization. They highlight that it needs to be fast, as they try to complete one diagnosis in one minute. Thus, one expert highlights the potential of online reformation capabilities, integrated with scanning equipment, for real-time processing in order to avoid delays.

- **Symmetric Visualization**: Viewing both breasts simultaneously is essential for comparison and detecting asymmetries. Symmetrical visualization supports thorough analysis and ensures that abnormalities are not overlooked.

Requirements List

The table below provides a summary of the requirements identified during the interviews. Radiologists are referred to as users U1 and U2, while the medical physics experts are denoted as E1 and E2. The items highlighted in bold will be the primary focus of this thesis. From the remaining three requirements: items 7 (automatic segmentation) and 8 (registration of sequences) are considered pre-processing steps in the visualization tool and item 14 (adjust windowing) is a standard feature for the user in the visualization tool.

Table 4.1: Summary of requirements based on interviews. Radiologists are represented as users U1 and U2, while medical physics experts are represented as experts E1 and E2. Bold items are the primary focus of this thesis.

ID	Type	Requirement	Description	Interview
T1	**Task**	**Scroll Through Slices**	Scroll through image slices to review detailed sections of breast tissue.	E1
T2	Task	Adjust Windowing	Adjust windowing settings to optimize contrast and brightness.	E1
T3	**Task**	**Annotate**	Annotate regions of interest within reformatted images for detailed evaluation and reporting.	E1, E2
T4	**Task**	**Measure Lesions**	Measure lesions accurately for assessment and preoperative planning.	U1, E1, E2
F1	**Feature**	**Automatic Reformation**	Automate the reformation of images to streamline the workflow for radiologists.	U1
F2	**Feature**	**Switch to Original Image**	Facilitate seamless switching between reformatted and standard view in order to retain contextual information.	U2, E1, E2
F3	**Feature**	**MIP**	Implement Thin MIP and 3D MIP to enhance visualization of subtle changes in breast tissue.	U1, E1, E2
F4	**Feature**	**Coronal Visualization**	Focus on coronal view for supine breast visualization, which also aligns with other clinical procedures.	U1
F5	**Feature**	**Whole Breast in One Image**	Allow for visualization of the entire breast in a single image or minimal slices to improve assessment efficiency.	U1
F6	**Feature**	**Annotation Transferred to Original Image**	Enable automatic transfer of annotations across different visualization views.	E1, E2
F7	Feature	Automatic Segmentation	Implement segmentation of breast tissue to remove irrelevant structures and enhance focus on areas of interest.	E1
F8	Feature	Registration of Sequences	Ensure registration of different imaging sequences for synchronized and cohesive viewing.	E1
F9	**Feature**	**Visualize Reformation Grid**	Visualize the reformation grid and allow for adjustment to fine-tune the visualization.	U2, E1
F10	**Feature**	**Rapid Image Processing**	Support rapid image processing to handle high volumes of cases and maintain workflow efficiency. Consider online reformation to enable real-time processing.	U1

CHAPTER 5

Visualization Design

This section describes the methods used in order to create the new visualizations, based on the literature review and user requirements.

5.1 Design Considerations

In response to the challenges and requirements presented in Section 3 and 4, we created two distinct prototypes for supine breast image reformation (F1), being the prerequisite for T1 (see 4.1). The selected methods are reflecting the main reformation approaches discussed in section 3:

- **Surface-Cutting Approach:** The first prototype, building on the corresponding state-of-the-art literature [34, 35, 40], will follow a "surface-driven approach". By leveraging a distance field to calculate offset surfaces, this prototype ensures that self-intersections are avoided. However, by calculating independent surface cuts, that are aligned in a post processing step, continuous pixel-wise correspondence between flattened individual cuts is not preserved.

- **Landmark Warp Approach:** The second prototype is inspired by the work of Obermann et al. [43], but introduces an automated flattening procedure and employs, instead of CPR, a volumetric deformation guided by anatomical landmarks. This method provides a continuous volumetric parameterization, similar in goal to the work of Abulnaga et al. [6]. However, as the breast shape can not be mapped to standard templates like planes or ellipsoids, our deformation is derived from control points along a breast segmentation.

This chapter will discuss these two prototypes in more detail, outlining the respective methodologies. First, the manual pre-processing steps are discussed, which are considered a prerequisite for the deformations.

35

5.2 Pre-Processing

Both reformation techniques share common pre-processing steps, described in this section. The requested features "Automatic Segmentation" (F7) and "Registration of Sequences" (F7), listed Table 4.1, were considered beyond the scope of this thesis. Consequently, these steps were performed manually. For the first approach, the segmentation followed the breast surface(see 5.1, left), whereas in the second approach, the rib cage was also included, masking all structures except for the breast tissue (see 5.1, right).

Figure 5.1: Breast segmentation for approach 1 (left) and approach 2 (right)

5.3 Approach 1: Surface-Cutting

Inspired by the work of Miao et al. [40] and Kretschmer et al. [34], who applied surface-based parameterization to flatten placenta and bone structures, this approach follows five main steps: (1) segmenting the breast, (2) generating a distance field from the segmentation, and (3) extracting iso-surface meshes at discrete distances, as shown in Figure 5.2.
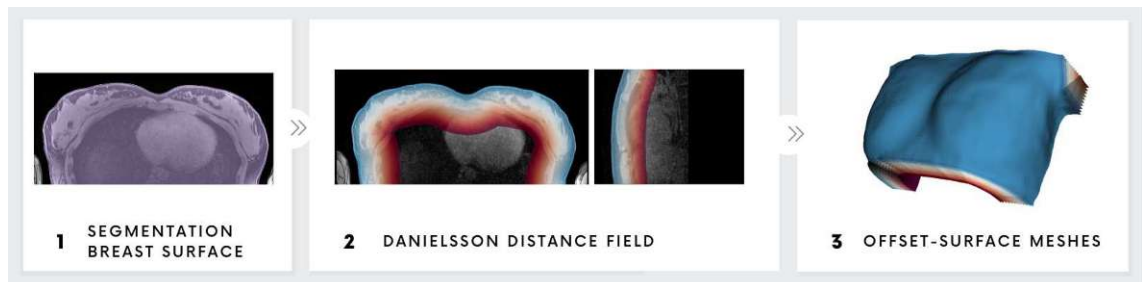
Figure 5.2: Overview surface cutting approach: Starting from a segmentation (1), a Danielsson distance field is computed (2), from which offset-surface meshes are extracted at fixed intervals (3).

Next, each extracted mesh is flattened individually (4), and the flattened meshes are stacked together to reconstruct a volume (5), which enables the possibility for users to scroll through layers in the usual fashion (T1 in Requirements 4.1). These steps are illustrated in Figure 5.3.

Figure 5.3: Overview surface cutting approach: Each surface is individually flattened using ARAP parameterization (4), then aligned and stacked to reconstruct a volumetric representation (5).

5.3.1 Distance Field

As first step for this approach, offset-surface meshes need to be created. One common way to generate these, is to displace the vertices of the initial surface mesh along their normal vectors [34]. However, as this technique can lead to self intersections, we use a Euclidean Distance Field as proposed by Miao et al. [40]. Specifically, we employ the method described by Danielsson [15], which computes the shortest Euclidean distance from each voxel to the segmented surface.

5.3.2 Offset-Surface Meshes

Once the distance field is computed, we extract offset surfaces by thresholding the field at discrete distance intervals. The choice of these intervals directly affects the quality and smoothness of the final flat volume. Given that our input data had a voxel spacing of $0.5 \times 0.5 \times 1$ mm, we first resampled it to an isotropic resolution of 0.5 mm. This oversampling step can help minimize sampling artifacts [34].

One important aspect to consider is the number of meshes to be extracted, as the distance field extends beyond the region of interest, reaching into the rib cage and interior of the body. As we are only interested in the breast tissue, we manually defined the maximum threshold, as depicted in Figure 5.4. In our data set, this maximum distance varied between 40 mm and 80 mm, depending on the individual breast.

The offset surfaces were then generated at discrete 0.5 mm intervals, corresponding to the underlying data and requirements raised in Section 4.2.5. Each extracted surface was subsequently triangulated and remeshed to ensure a uniform distribution of vertices. To achieve this, we applied Voronoi-based clustering for remeshing, following the method described by Valette and Chassery [67].

5.3.3 Flattening

The aim of parameterization is to establish a bijective mapping that preserves specific properties of the original surface as accurately as possible. This preservation can focus on angles (conformal), areas (equiareal), and/or lenghts (isometric) [33, 35].

37
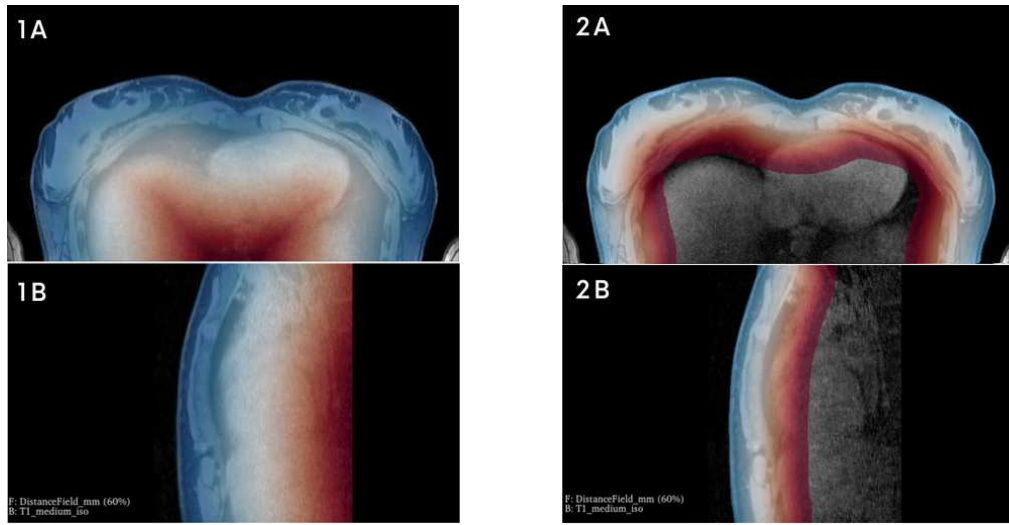
Figure 5.4: Full extent (1) and used range (2) of the Danielsson Distance Field, visualized on axial and sagittal breast slice view [15].

For our surface mapping, we employ a As-Rigid-As-Possible (ARAP) parameterization, through the adoption of a local/global algorithm, introduced by Liu et al. [35]. ARAP prioritizes area preservation and aims for isometry, which makes it very effective for shape-preserving parameterizations. Liu et al. [35] mention that this can potentially come at cost of conformality, however in their observation the area preservation came at a very small, even insignificant, penalty of angle distortion compared to other approaches. Their approach iteratively alternates between computing locally optimal rotations for each triangle and globally optimal 2D coordinates to minimize deformation energy. The implementation details can be found in the work of Liu et al. [35]. Figure 5.5 shows the result of this parameterization process of a breast surface mesh. A sparsely sampled mesh is used here for illustrative purposes, while in our prototype, we employ a denser mesh with 100,000 vertices to ensure high-quality deformation.
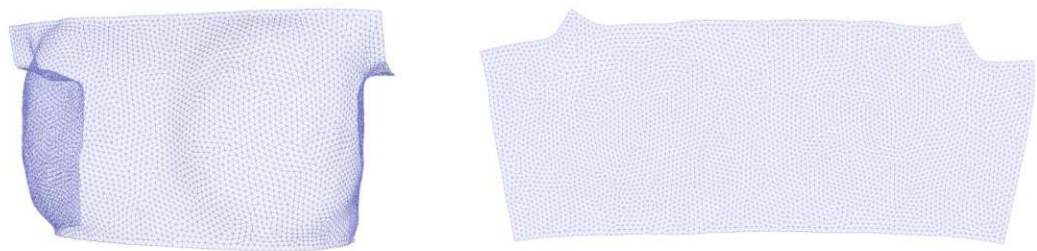
Figure 5.5: Triangulated original mesh (left) and ARAP-parameterized mesh (right) [35].

5.3.4 Post-Processing

After each mesh was flattened, the individual meshes needed to be combined to a volume, in order for users to scroll through the slices in the usual fashion (T1 in Requirements 4.1). Since ARAP prioritizes the preservation of angles and lengths within each mesh independently [35], the resulting individual flat offset-meshes are not aligned (see Figure 5.6, left).

To address this, we applied a Orthogonal Procrustes Analysis (OPA) [18], aligning each mesh to the first reference mesh. We used rotation and translation only, explicitly excluding scaling to preserve the relative size differences introduced by the distance field. Thus, rotation and translation is performed while ensuring that the triangle sizes remain unchanged. Following the mesh alignment, each mesh was offset in the coronal direction by the 0.5 mm discrete distance used for slicing earlier ("stacking"), ensuring that each offset mesh aligns with the correct coronal layer. This is illustrated in Figure 5.6, right.

FLAT MESHES BEFORE PROCRUSTES ANALYSIS

FLAT MESHES AFTER ALIGNMENT & STACKING

0.5mm
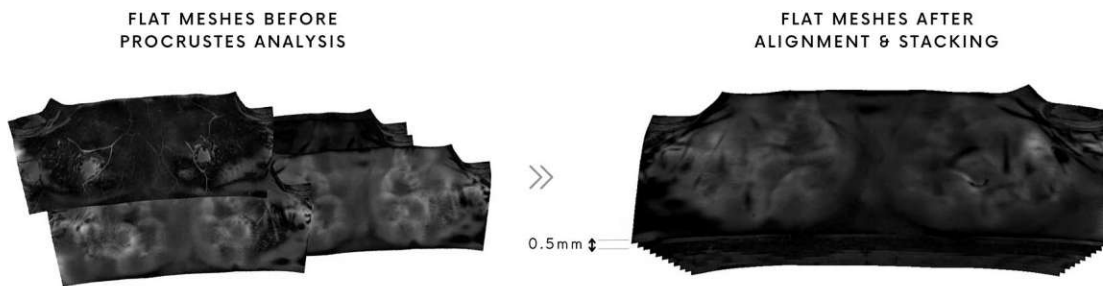
Figure 5.6: Reconstruction of a volumetric representation by stacking flat meshes.

To ensure a correct orientation along the axes, we then aligned the combined meshes using Principal Component Analysis (PCA) [66]. PCA is a statistical technique, that identifies the principal axes of variation in a dataset. In the context of our flattened meshes, PCA helps determine the dominant geometric directions, allowing for global alignment and ensuring that the final volume is consistently oriented. We used PCA because it provides a simple, efficient and data-driven method to derive the global orientation directly from the shape geometry [66]. For the PCA, first, the centroid of the combined mesh was computed to shift the points to the origin. Then, the covariance matrix of the point coordinates was computed, and eigenvalue decomposition was performed on this covariance matrix. This provided the eigenvectors (principal components), which indicate the directions of maximum variance. Finally, these principal components were used to determine the rotation required to align the mesh with the coordinate axes.

After the alignment process, the flattened meshes needed to be converted back into a volumetric representation to allow users to navigate through the slices in a conventional manner. To achieve this, we resampled the stacked 2D mesh data into a 3D structured grid, as described in the work of Schroeder et al. [56]. For each point in the volume, the corresponding location in the stacked meshes is identified, and interpolation weights are

computed to estimate the data values at that location. The interpolation [56] can be described as follows:

$$d = \sum_{i=0}^{n-1} W_i d_i$$

where d is the interpolated value at a given point, d_i are the known values at the cell's vertices, and W_i are the interpolation weights that depend on the parametric coordinates (r, s). The weights satisfy the following constraints:

$$\sum_{i=0}^{n-1} W_i = 1, \quad 0 \leq W_i \leq 1$$

ensuring that the interpolated value remains within the range of the original data points. The interpolation is performed using barycentric coordinates (r, s), defining the point's relative position within the triangle. The corresponding weights are given by $W_0 = 1 - r - s, \quad W_1 = r, \quad W_2 = s$, where W_0, W_1, W_2 are the interpolation weights corresponding to the vertices P_0, P_1, P_2 of the triangle.

5.3.5 Navigation Design

To facilitate spatial orientation within the parameterized volume, we implemented a navigation aid that establishes a direct correspondence with the original reference image. For this we use the current slice index of the coronal slider to dynamically threshold the initial distance field. This thresholded region is then overlaid onto the original image to provide a visual reference for navigation (see green line in Figure 5.7).
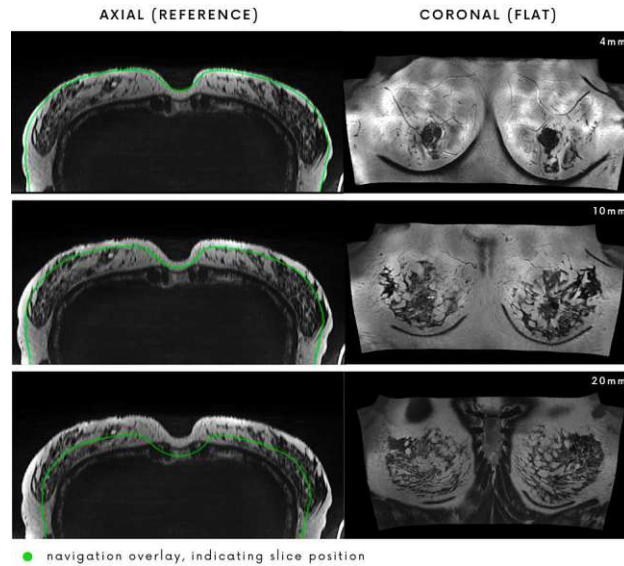
Figure 5.7: Navigation aid: the left image shows the original images with the green reference line, the right images shows the corresponding coronal slice in the flat volume.

5.4 Approach 2: Landmark Warp

For the second approach we employed a landmark warp based on pre-defined control points. This approach follows four main steps: (1) segmenting the breast, (2) creating control points based on the rib cage curvature, (3) paramterize the curves to create target points, and (4) applying the deformation through a TPS transform. These steps are illustrated in Figure 5.8 and described in this following section.
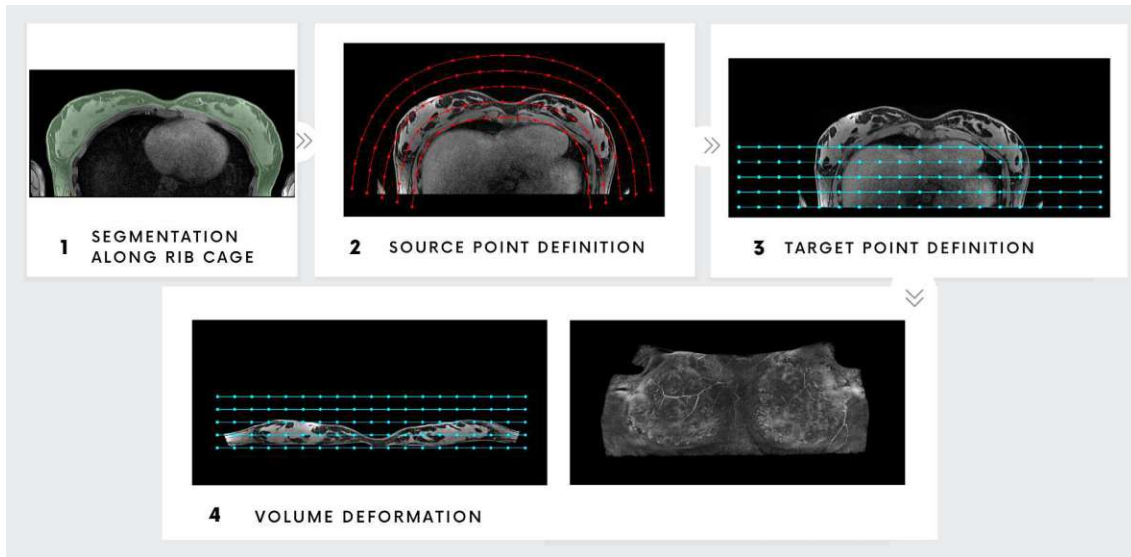
Figure 5.8: Overview of the landmark warp approach. Starting from a segmentation (1), control points are defined along the rib cage (2) and parameterized by arc length (3). These corresponding point sets serve as input for a volumetric deformation (4).

5.4.1 Landmark Extraction

Similar to the first approach, this method is based on an initial segmentation. However, in this case, the segmentation contains only the breast and ends along the rib cage (see 5.1, right and 5.8, step 1). To define the deformation transform, we first extracted source and target control points from the segmentation, based on the contours (see Figure 5.9).

Source Control Points

For the source control points (Figure 5.8, step 2), we analyzed the axial slices and extracted contours using the Marching Squares algorithm [36]. From each slice, we selected the two longest contours and labeled them as inner or outer (see Figure 5.9, red and blue), based on their distance to the lower image centroid ($[X/2, 0]$). The inner contour was smoothed using a cubic spline to avoid sharp corners and self-intersections, which ensures more accurate normal projections in the next step. We then projected points from the inner contour outward along its normals to measure the maximum
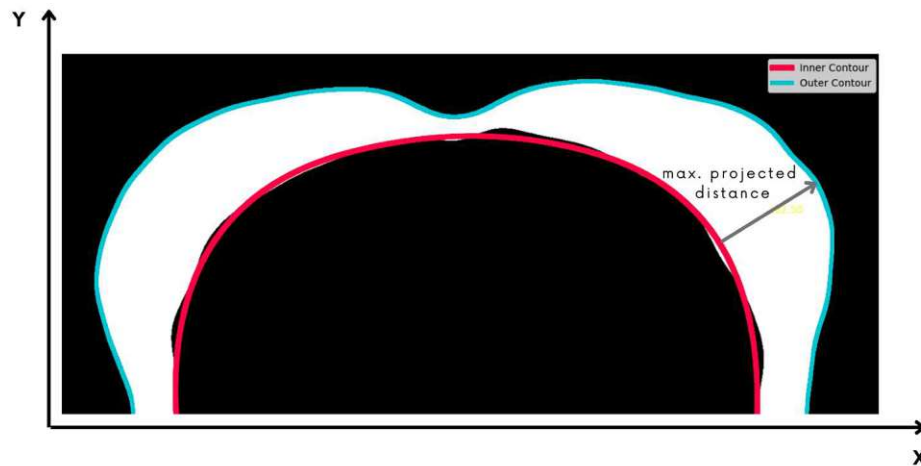
Figure 5.9: Determination of source control points and breast tissue extent from contours. The inner contour, following the rib cage (red), the outer contour following the breast shape (blue) and the projected distance.

distance to the outer contour. Figure 5.9 shows this distance calculation based on one axial slice, we repeated this for all axial slices to determine the overall maximal distance. Based on this distance, we created offset copies of the inner contour, extending outward until the maximum range was covered (see step 2 in Figure 5.8 for the red offset curves).

Each curve is also offset i times along the z-direction, based on the sternum's shape (illustrated in Figure 5.10). The number of copies i, can be customized through the user. The sternum's height at each slice is defined by the inner contours extracted from the axial slices.
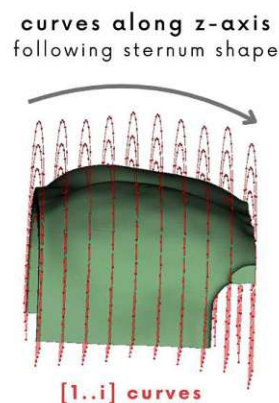
Figure 5.10: Curves in z-direction, following the sternum shape.

Target Control Points

To determine the target control points (Figure 5.8, step 3), we parameterized the curves using two approaches. The first approach preserved the arc length of each contour individually. However, this method introduced high distortions between layers, as illustrated in Figure 5.11, B on the example of a 2D checkerboard image. In the second approach, all contours were re-scaled uniformly based on the length of the middle curve (Figure 5.11, C). We selected the second method as our final approach due to its lower distortion across all measured metrics (see Table 5.1).
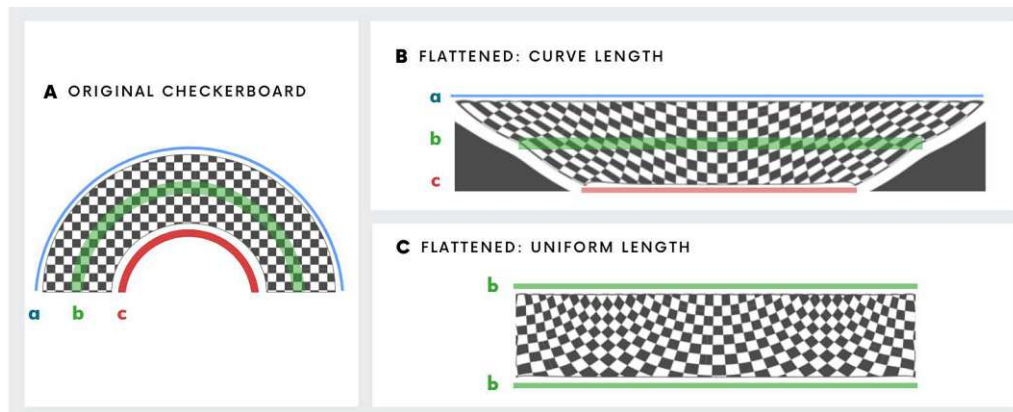
Figure 5.11: Evaluation of target points in 2D: (A) Preserving individual arc lengths, (B) Using uniform length based on the middle contour.

Figure 5.12: Comparison of flattening approaches: Preserving individual arc lengths (left), Using the middle contour for uniform scaling (right).

Table 5.1: Comparison of distortion metrics for target control points. All values are relative distortions measured in $\log_2$ scale.

Metric	Individual Arc Lengths	Uniform Middle Length
Average Metric Distortion	0.12	0.09
Average Area Distortion	0.17	0.14
Average Distance Distortion	0.078	0.052

The total length of each curve C is computed by discretizing the spline into a set of points and summing the Euclidean distances between consecutive pairs. This method, based on cumulative chordal distance [7], provides a numerical approximation of the curve's arc length. In our implementation, we evaluated each spline at $N = 1000$ uniformly spaced parameter values to ensure sufficient accuracy. The total length L is then approximated as:

$$L \approx \sum_{i=1}^{N-1} \|\mathbf{C}(u_{i+1}) - \mathbf{C}(u_i)\|_2 \tag{5.1}$$

where $\mathbf{C}(u_i) = (x_i, y_i)$ are the evaluated spline points, evenly spaced across the curve, and $\|\cdot\|_2$ is the Euclidean norm.

Using the resulting arc length parameterization, each curve is then divided into a user-defined number of evenly spaced points, n, which are specified via the prototype interface. These n samples form the source control points and their corresponding target control points used in the transformation process described in the following section. Step 2 of Figure 5.8 shows the source control points, while Step 3 illustrates the parameterized target control points. For clarity in the illustration, we used 19 points.

5.4.2 Volumetric Transformation

For the warping process (Figure 5.8, step 4), meaning deforming the volume based on the defined control points, we used a Radial Basis Function (RBF)-based transformation within the Thin Plate Spline (TPS) framework. We chose a TPS transformation because it is computationally efficient, produces smooth interpolations, and is well-suited for user interaction given the control points. This aspect is particularly relevant in clinical applications, where physicians prefer to keep control over the results [55], which also emerged as a requirement from our user interviews (see F9 in Table 4.1). TPS were first introduced in image analysis for landmark-based image registration by Bookstein et al. [11], where they were used to compute deformation fields from scattered data samples. TPS have a physical motivation of minimizing bending energy and provide a closed-form solution for mapping a set of corresponding points in different images while ensuring a smooth transformation [55,70]. The underlying mathematical formulation and implementation details of the TPS are described in detail by Donato and Belongie [17].

However, one limitation we noticed is the local influence of the control points. This is especially visible when quantifying distance distortions of the neighboring cells (see Figure 5.13, left). According to Rohr and Wörz [55], this limitation stems from the mathematical formulation of TPS, where control points act as point forces, resulting in an infinitely small support region for each force. Consequently, the influence of each landmark does not propagate smoothly across the entire image, leading to spatially inconsistent transformations. This can be problematic for our case of breast MRI warp, where a uniform deformation is desired.

Therefore, while TPS is commonly associated with the RBF $U(r) = r^2 \log r$ [17], we explored setting an alternative RBF. Specifically, we tested the multiquadric RBF [59], defined as:

$$U(r) = \sqrt{1 + (\epsilon r)^2} \tag{5.2}$$

where ϵ is a shape parameter that controls the smoothness and spread of the deformation. We fixed $\epsilon = 1$ based on empirical testing, selecting a value that consistently produced smooth and visually coherent deformations in our use case (see Figure 5.13, right).

Figure 5.13: Deformed volume showing relative distance distortion: Standard TPS transform (left) compared to TPS transform with multiquadric RBF function (right)

5.4.3 Navigation Design

In this approach spatial context is provided through a visual grid showing source and target points overlaid on each slice (Figure 5.8, step 2-4) and the 3D volume (Figure 5.14). This feature directly responds to one user requesting the ability to view and optionally adjust the deformation grid (F9 in Requirements 4.1). The landmark warp method is particularly well-suited for this: unlike approach 1, which flattens layers individually and lacks a global deformation model, approach 2 applies a continuous volumetric deformation. This enables seamless correspondence between the original and reformatted representations. The prototype further supports interaction by allowing users to modify the source points prior to deformation.
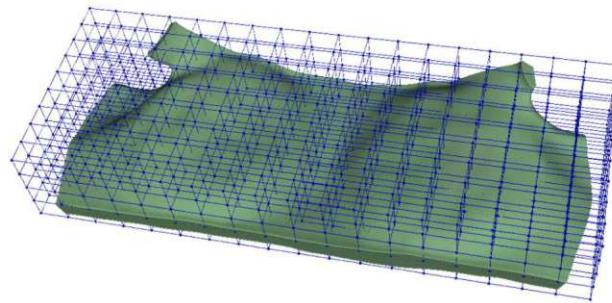
Figure 5.14: Visualization of landmark warp target grid as 3D overlay.

5.4.4 Annotations

Additionally, the interviews highlighted the need for annotations in regions of interest for evaluation and reporting (T4 and F6). This was implemented in the second prototype (see Figure 5.15), where the continuous volumetric deformation enables consistent mapping between the original and flattened images. Annotations placed in one view are automatically transferred to the other. We used a cross symbol as a 2D glyph to avoid obscuring the underlying structure. The prototype also allows for measuring (T3) on the flattened image, which can be transformed back to the original image.
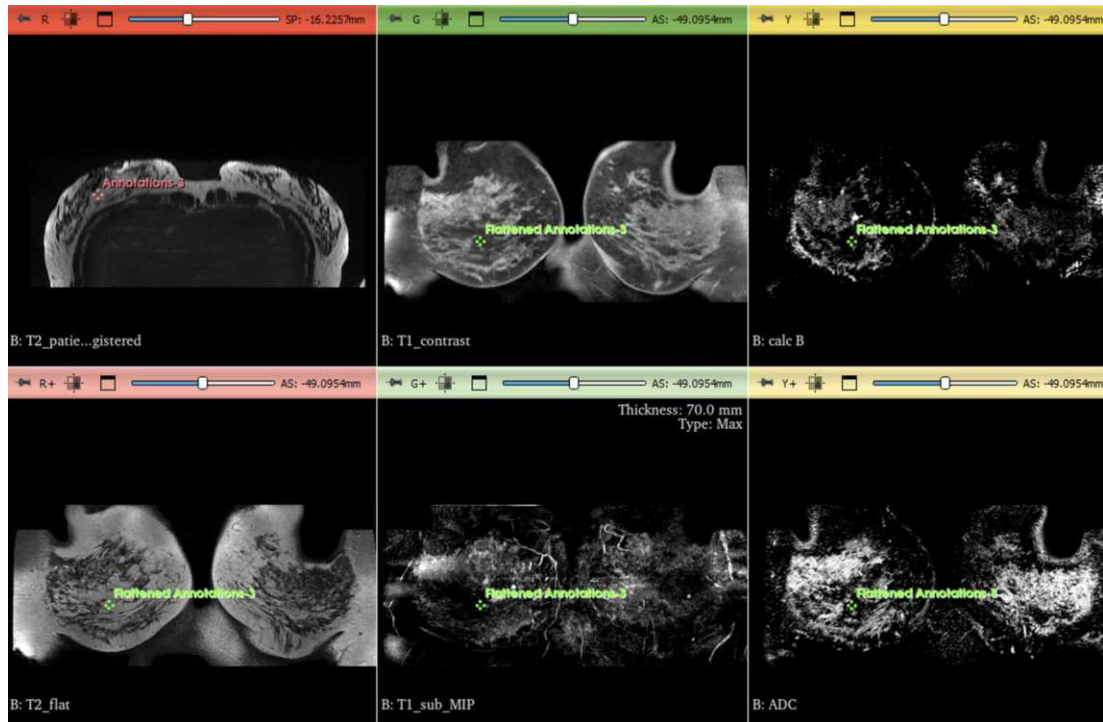
Figure 5.15: Synchronized annotations for the landmark warped volume, showing an original axial slice (top-left) and five deformed slice views.

CHAPTER 6

Implementation

This section describes the technical details of our implementation, including the used software frameworks and libraries. We implemented our methods using a combination of Python and C++. The flattening pipeline was executed on an AMD Ryzen 9 7950X3D 16-Core CPU and an NVIDIA GeForce RTX 4080 GPU. We integrated both of our prototypes as plugins within 3D Slicer [1, 20] to enable direct integration with other imaging modules within the software. 3D Slicer is an open-source platform for medical image analysis and visualization. It provides support for VTK and ITK, which made it well-suited for our implementation. As noted in Section 4, 3D Slicer also provides additional plugins that address tasks outside the scope of our implementation. These include modules for sequence segmentation (see Table 4.1, F7), registration (F8), and a standard feature for windowing adjustments (T2). For manual segmentation, we utilized the "grow from seeds" feature in 3D Slicer's segment editor [46]. For image preprocessing, we used the 3D Slicer Elastix implementation [32, 57] for registration, along with the Plastimatch deformable B-Spline Registration module [47] included in 3D Slicer.

6.1 Approach 1: Surface-Cutting

Approach 1 was partially implemented in 3D Slicer using Python, while some components, particularly for parameterization, were handled in C++. For the distance field creation, we used the `DanielssonDistanceMapImageFilter` provided by the ITK library [29]. Then, we used `vtkDiscreteFlyingEdges3D` to extract the surface from the mask. This resulted in a `vtkPolyData`, which was cleaned and triangulated. The pyvista [61] and pyacvd [5] libraries were employed for clustering and remeshing, and the final mesh was exported as a VTP file. Parameterization was done using the C++ library CGAL [3] with the ARAP parameterizer [35]. Once the flat meshes were obtained, we performed alignment using OPA and PCA, again with Python. The final volume reconstruction was carried out using a `vtkProbeFilter` [56].

6.2 Approach 2: TPS Warp

The TPS Warp approach was fully implemented in Python as a dedicated plugin within 3D Slicer [1, 20], depicted in Figure 6.1.
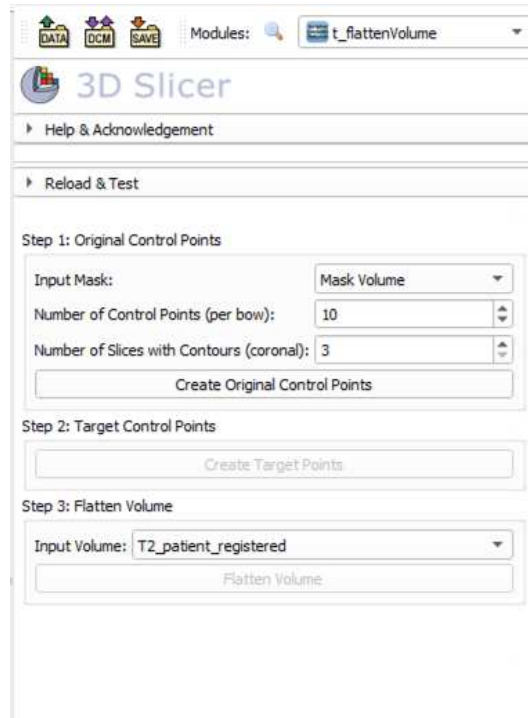
Figure 6.1: 3D Slicer plugin for the landmark warp approach. Takes a mask volume and the number of source control points as input. Subsequently, the target control points can be generated and a user-defined breast volume can be flattened.

We used the skimage library [68] to extract contours from the input images, VTK [56] was used for the remaining operations. The 3D Slicer MRMLCurveNodes were utilized to visualize and adjust control points interactively. As described in the previous section, the volume warping was performed using vtkThinPlateSplineTransform, with a custom radial basis function. The resulting transformation was stored as a vtkMRMLTransformNode, allowing users to map measurements in the flattened space back to the original image. For the volume rendering and creation of the volume MIP and thin MIP, we also used the modules available in 3D Slicer [1, 20].

CHAPTER 7

Evaluation and Results

7.1 Quantitative Evaluation

Deformation inevitably introduces distortions [34], which need quantification in order to evaluate the accuracy of the approaches. In this section, we first define the metrics used to assess the distortions, before presenting the evaluation results across the two proposed methods.

7.1.1 Evaluation Methods

All distortion metrics are reported in a $\log_2$ scale, where a value of 1 indicates a doubling of local distance or area, 0 means no change, and negative values indicate compression. In addition we provide measures on the average time performance of the reformation process for each method. To evaluate the techniques across a representative range of breast sizes, we measured distortion using data from three healthy subjects described in Section 2.4, categorized as small, medium, and large.

Inspired by the work of Abulnaga et al. [6], we compute the area distortion and metric distortion to evaluate how well each approach preserves shape properties. The surface-cutting approach is based on a mesh, while the landmark warp operates on a quadrilateral volume. In order to compare them we extracted the surface mesh from the volume and also flattened it using the landmark warp. We then compute the distortion metrics for both methods based on the surface mesh.

The area distortion of one triangle is calculated through $\log_2\left(\frac{\hat{A}_m}{A_m}\right)$ where A_m is the area of triangle m in the original mesh, and $\hat{A}_m$ is the area of the corresponding triangle in the flattened mesh [6]. To obtain a global measure, we compute the average of the distortion

49

of all triangles of the mesh as:

$$average\_area\_distortion = \frac{1}{N} \sum_{m=1}^{N} \left| \log_2 \left(\frac{\hat{A}_m}{A_m} \right) \right| \tag{7.1}$$

where N denotes the total number of triangles.

Similarly, metric distortion is calculated through $\log_2 \left(\frac{x_{ij}}{z_{ij}} \right)$ where zij is the length of edge (i, j) in the original mesh and x_{ij} is the length of the same edge in the flattened mesh [6]. As with area distortion, the average metric distortion over the entire mesh is computed as:

$$average\_metric\_distortion = \frac{1}{M} \sum_{i,j} \left| \log_2 \left(\frac{x_{ij}}{z_{ij}} \right) \right| \tag{7.2}$$

where M is the total number of edges.

For the volumetric transformation of the second approach, we compute an additional distortion metric. We evaluate distance distortion inspired by the work of Rist et al. [54] and [63] to quantify how much the relative distances between neighboring points in the 3D space change after the transformation. For the calculation we convert the volume to a `vtkPolyData`, and use KD-trees to extract the k-nearest neighbors. For each point i, and each neighbor $j \in \mathcal{N}(i)$, we compute the Euclidean distance $||\mathbf{x}_i - \mathbf{x}_j||$ in the original space and $||\hat{\mathbf{x}}_i - \hat{\mathbf{x}}_j||$ after transformation. We then compute the mean log ratio over each point's neighborhood:

$$d_i = \frac{1}{k} \sum_{j \in \mathcal{N}(i)} \log_2 \left(\frac{||\hat{\mathbf{x}}_i - \hat{\mathbf{x}}_j||}{||\mathbf{x}_i - \mathbf{x}_j||} \right)$$

Globally, we report the average across all points through:

$$average\_distance\_distortion = \frac{1}{P} \sum_{i=1}^{P} |d_i| \tag{7.3}$$

where P is the total number of points in the volume.

7.1.2 Evaluation Results

Approach 1: Surface-Cutting

For the surface-cutting approach, we analyzed metric and area distortions per surface and offset mesh across different breast sizes. The results are listed in Table 7.1 and Figure 7.1, showing three different breast sizes at three different offset distances. All meshes in this analysis were sampled to 100,000 vertices. The offset distances represent the distance in millimeters from the original surface, where 0 mm is the original surface mesh.

This shows up that both metric and area distortions tend to increase with breast size. The small breast ($\approx$ 600 ml) exhibits the least distortion (Figure 7.1, first row), while the large

Table 7.1: Quantitative comparison of metric and area distortion across three breast sizes and offset distances for approach 1. Distortion values are relative measures in $\log_2$ scale; durations indicate parameterization time per mesh in seconds.

Offset Distance	Breast Size	Metric Distortion	Area Distortion	Duration per mesh
0 mm	Small	0.030	0.052	63.3 s
0 mm	Medium	0.035	0.062	62.4 s
0 mm	Large	0.034	0.061	60.5 s
20 mm	Small	0.033	0.057	63.9 s
20 mm	Medium	0.044	0.075	63.1 s
20 mm	Large	0.043	0.074	59.9 s
40 mm	Small	0.033	0.055	66.5 s
40 mm	Medium	0.048	0.079	63.6 s
40 mm	Large	0.049	0.081	63.4 s
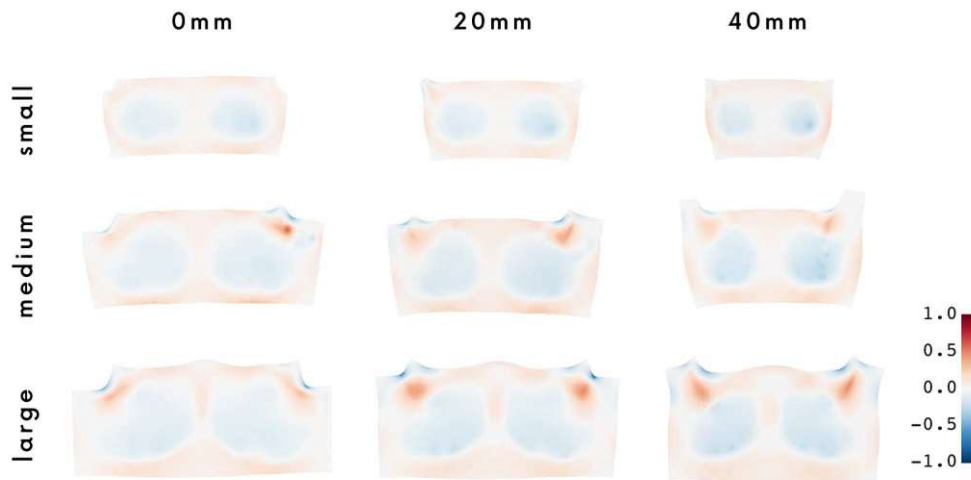
Figure 7.1: Logarithmic area distortion visualized across different breast sizes and offset distances. Distortion tends to increase with breast size and distance from the surface.

breast (≈ 3000 ml) shows the highest values (Figure 7.1, last row). The overall distortion remains relatively low, with the metric distortion ranging between 2.1% to 3.5%, and the area distortion between 3.7% and 5.8% when converted from the logarithmic scale. Distortion values vary slightly across different offset distances. As the distance from the surface mesh increases, the distortion increases as well. This is for example visible in large breasts, where the metric distortion increases from 0.034 on the surface mesh to 0.049 at a depth of 40mm (from 2.4% to 3.5%). As noted in the previous section (see 5.3.2), we adjusted the maximum required depth manually based on breast size, with small breasts requiring a maximum depth of 45mm.

The average processing time for a single mesh was approximately one minute. Including average 18 seconds of pre-processing (specifically, distance field computation and re-meshing to 100,000 vertices), the total time per mesh was approximately 78 seconds. As a result, reformatting a full breast volume into 50 slices with 1mm spacing required around 65 minutes in total. To explore faster alternatives, we conducted preliminary tests using sparsely sampled meshes with 5,000 vertices. The tests were performed using the surface mesh; Table 7.2 compares results across different breast sizes for both high- and low-resolution meshes. We observed a substantial reduction in parameterization time (e.g., from 63.58s to 1.21s per mesh) and when adding the same 18s of pre-processing, the total time per mesh dropped to approximately 19.21s. This would reduce the total runtime for 50 meshes to about 16 minutes. However, this comes at the cost of increased metric and area distortion, indicating that higher-resolution meshes preserve geometric accuracy better. For our final prototype implementation, we therefore used the high-resolution meshes with 100,000 vertices. We need to note here that the focus of this work was not at optimizing these values and further improvements for pre-processing and flattening are likely possible through parallelization and GPU acceleration.

Table 7.2: Comparison of metric and area distortion for low-resolution (5k vertices) and high-resolution (100k vertices) surface meshes across different breast sizes. Distortion values are relative measures in $\log_2$ scale; duration is given in seconds per mesh.

Breast Size	Vertices	Metric Distortion	Area Distortion	Duration per Mesh
Small	5,000	0.036	0.070	1.21 s
Small	100,000	0.030	0.052	63.3 s
Medium	5,000	0.045	0.087	1.21 s
Medium	100,000	0.035	0.062	62.4 s
Large	5,000	0.048	0.094	1.21 s
Large	100,000	0.034	0.061	60.5 s

7.1.3   Approach 2: Landmark Warp

To evaluate the approach, we applied the landmark warp across different breast sizes. One challenge when using landmark warp was to balance the number of control points (described in Section 5.4.1). Generally, we tried to keep the number of points as low as possible in order to reduce computation time but still ensure a satisfactory transformation. We tested multiple configurations, varying both the number of control points n per curve and the number of curves i in the z-direction (along the sternum shape). As illustrated in Figure 7.2, using too few control points (e.g., $n = 10$ in example a) resulted in visible local deformations. In contrast, increasing the number of control points improved the smoothness and uniformity of the transformation. Using $n = 30$ control points per curve (example c) yielded noticeably better results and a smooth transformation in our tests. Based on this observation, we chose $n = 30$ for the final prototype.
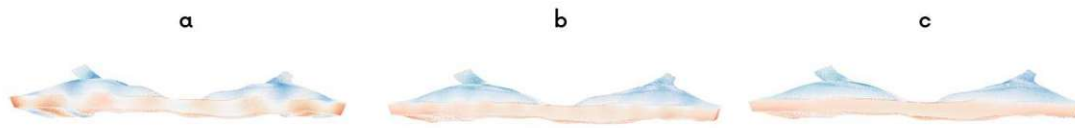
Figure 7.2: Effect of control points on TPS transform: (a) 10 points, (b) 20 points, (c) 30 points n per axial curve.

For the number of curves i, we found while while 3 curves were sufficient to flatten the ribcage, 4 curves could improve the accuracy of the deformation, as the points followed the sternum more closely (see visual assessment in Figure 7.3). Table 7.3 presents the distortion metrics for both configurations. However, more curves did not necessarily reduce overall distortion. In regions with high curvature along the ribcage, the additional points introduced more localized adjustments, increasing distortion in neighboring areas. ncreasing the number of control points also increased computation time. Additionally, more curves resulted in longer computation times. Nonetheless, we proceeded with 30 control points (n) per curve across 4 slices (i) in our final implementation, as this configuration provided a good balance between deformation quality and computational efficiency.
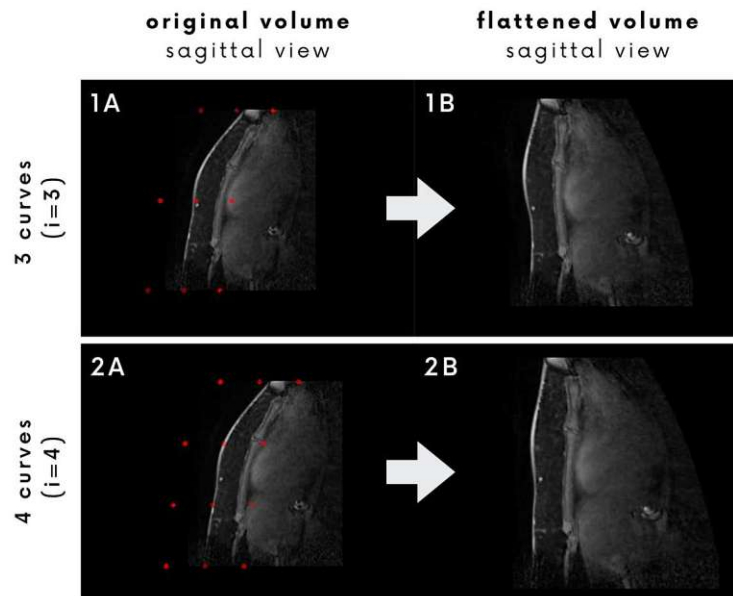
Figure 7.3: Curves i along sternum of the large breast. The flattening using 3 curves (1A, 1B) was more efficient, but 4 curves reflect the sternum shape more accurately (2A, 2B).

Similar to the first approach, the distortion increased with breast size. Figure 7.4 shows the average distance distortion across different breast sizes. In this second approach, also the computation duration in increased with breast size. Using a uniform length, based

Table 7.3: Quantitative evaluation of metric, area, and distance distortion across different breast sizes and numbers of control curves (i) for approach 2. Each configuration uses $n = 30$ control points per curve. Distortion values are given in $\log_2$ scale; duration is reported in seconds per volume.

Breast Size	Nr of curves i	Total Points	Metric Distortion	Area Distortion	Distance Distortion	Duration per vol.
Small	3	270	0.044	0.080	0.019	32.27 s
Small	4	360	0.043	0.081	0.021	40.13 s
Medium	3	270	0.086	0.143	0.036	164.79 s
Medium	4	360	0.081	0.139	0.037	218.22 s
Large	3	270	0.129	0.196	0.055	221.59 s
Large	4	360	0.130	0.208	0.063	343.52 s

on the middle length, for flattening the breast caused increased distance distortion at the lower and upper part, but relatively low in the middle (see Figure 7.4, left column). Table 7.3 shows that the metric distortion for a medium-sized breast surface is 0.081, corresponding to a 5.8% change in surface edges. However, the distance distortion across the entire volume was smaller, with a value of 0.037, indicating a 2.6% change in neighborhood distances. For smaller breasts, the total deformation process took only 40.13 seconds, while for larger breasts, the process required approximately 5.5 minutes. The preprocessing step, which involved computing control points, was quick, taking about 1 second on average. Since the process operated directly on the volume, no post-processing was necessary for this approach.
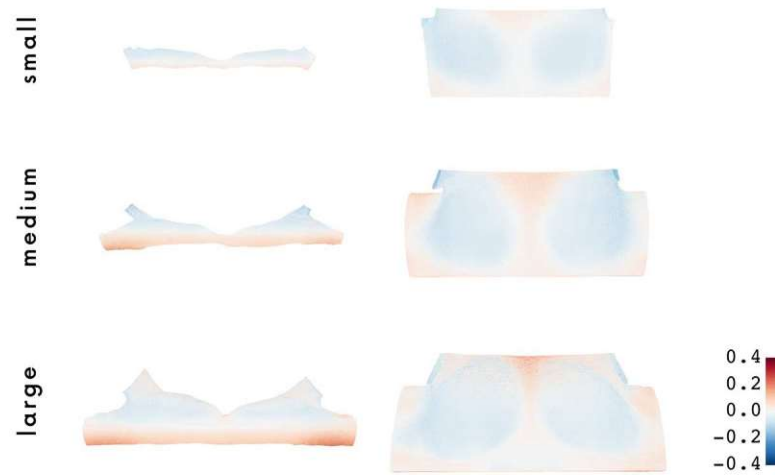
Figure 7.4: Average distance distortion across breast sizes and views (inferior left, anterior right). Rows show small, medium, and large sizes, with distortion on a $\log_2$ scale.

Comparison of the Approaches

Both methods showed increasing distortion with breast size. Figure 7.5 visualizes the comparison of the logarithmic area distortion of the surface mesh across different breast sizes. Overall, the first approach inhibits less distortion on the surface mesh, especially with increasing breast size (see last row in Figure 7.5). This is not surprising, as the underlying method, ARAP, is a mesh-based parameterization focused on preserving local rigidity [35]. However, as noted before, the distortion of the individual meshes can increase slightly at offset meshes across different distances. In contrast, the second approach exhibits higher distortion at the surface but preserved the volumetric structure better, resulting in low average distance distortion across the full volume (see Figure 7.4).
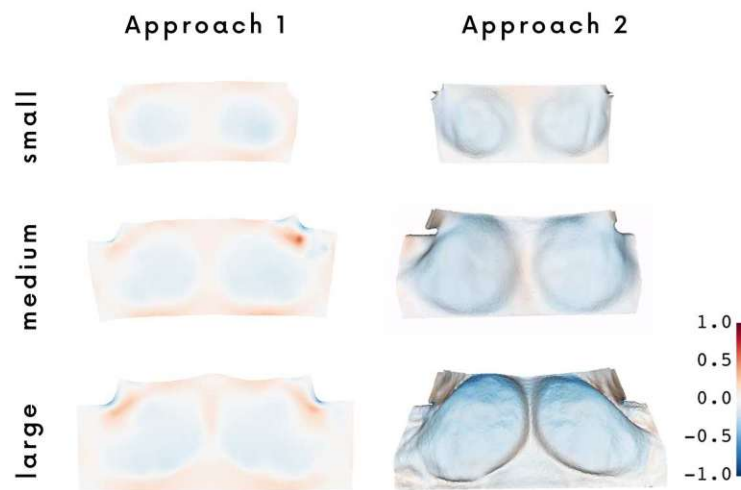
Figure 7.5: Comparison of $\log_2$ area distortion of surface-cutting approach (left) and landmark-warp approach (right) based on the surface mesh. Approach 1 inhibits less distortion on the surface mesh. Distortion increases with breast size for both approaches.

When considering runtime (see F10 in 4.1), the second approach proved faster than the first in our tests. As shown in Table 7.3, the processing time for the landmark warp method increased with breast size, ranging from approximately 40 to over 340 seconds. In contrast, the first approach required significantly longer processing times of up to 60 minutes due to the individual parameterization of high-resolution meshes with 100,000 vertices. Preliminary tests using sparsely sampled meshes with 5,000 vertices reduced per-mesh processing time from 63.58s to 1.21s, suggesting significant performance gains are possible.

In terms of practical impact (see F2 in 4.1), both approaches significantly reduced the number of slices containing breast tissue. While radiologists typically review axial slices in MRI workflows, the proposed flattened visualizations present tissue in a coronal view, enabling an overview of the breast in fewer slices. For example, in a case with 0.5 mm isotropic spacing, the original 384 axial slices (see Figure 7.6, top row) were reduced to

94 coronal slices using surface-cutting and 123 slices using landmark-warp (Figure 7.6, bottom row). This aligns with prior findings [43], suggesting that flattened views can reduce reading times for supine breast MRIs. As future work, a larger quantitative study involving radiologists will be needed to confirm and quantify the observed reduction in reading times.
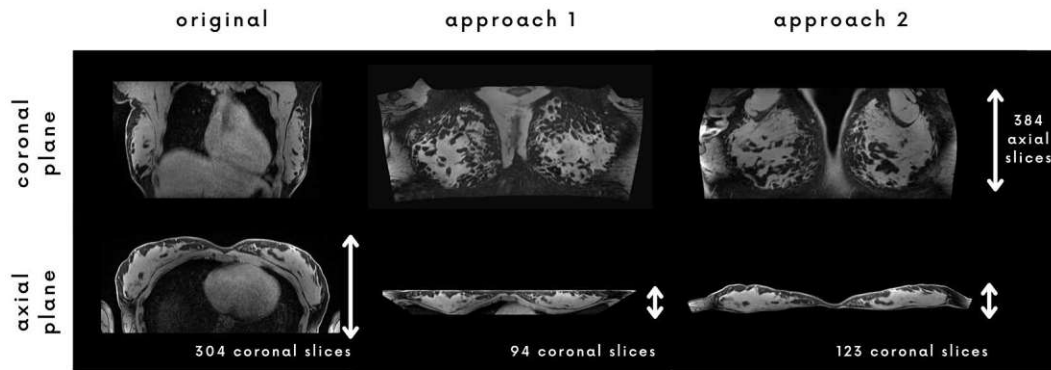
Figure 7.6: Comparison of slice reduction between original and flattened views. Top row: Coronal view, with the number of axial slices (384 slices at 0.5mm spacing). Bottom row: Axial view, with the number of coronal slices required.

7.2 Qualitative Evaluation

To assess the effectiveness of the developed prototypes in supporting lesion detection and diagnosis, we conducted a qualitative evaluation with radiologists and medical physics experts. All participants were shown two initial setups, which demonstrated the deformation methods, with a reference view in all axes (axial, sagittal and coronal). In these setups, we used the T1-weighted medium-sized breast (see Chapter 2.4 for details on the dataset), as this breast size exhibited the most balanced distortion, discussed in the previous Section 7.1. The radiologists were additionally presented a third setup simulated a realistic diagnostic scenario, with patient data, to facilitate a direct comparison of both approaches mimicked in a real-world scenario. Since our focus was on evaluating the visualizations rather than the user interface, we presented only the visualization prototypes rather than demonstrating the plugins themselves.

7.2.1 Evaluation Methods

The evaluation followed a similar approach to the initial interviews, using semi-structured interviews. This time we combined the interviews with a "think-aloud protocol" inspired by Carpendale [13] and Preim et al. [51]. Participants were encouraged to follow their typical workflow for lesion inspection, especially in the third setup, and asked to verbalize their thoughts. This method aimed to capture real-time impressions as participants interacted with the visualizations. The collected data was analyzed using thematic analysis, as described by Braun and Clarke.

Recruitment and Participants

The same four participants from the initial interviews were recruited for the final evaluation of the visualizations. As described in Section 4.1, two were radiologists and two were medical physics experts specializing in magnetic resonance imaging. While re-engaging the same participants could introduce some bias due to their familiarity with the project, it also ensured that the evaluation remained focused on the specific requirements identified earlier, allowing us to assess how effectively those needs were addressed.

Data Collection

Our data consisted of audio-recorded interviews, screen recordings, and handwritten notes taken by the interview leader. The interview questions focused on evaluating the main research question of this thesis: *To what extent can a flattening-based visualization method improve the clinical utility of supine breast MRI?* Participants were encouraged to speak out their thoughts and were then in each setup asked additional questions about perceived distortions, the intuitiveness of the visualization and potential improvements over current methods. In the end we prepared an additional semi-structured interview guide to get their overall feedback (see Appendix C).

Procedure

The procedure was identical to the interviews (see Section 4.1), except that we additionally recorded the screen so we could analyze the way the radiologists interacted with the different setups in more detail. The procedure was done in German and the direct citations were translated from German for the following analysis. Before the interviews were conducted, all participants signed an informed consent form, which also included a data protection agreement.

7.2.2 Setup 1: Surface-Cutting

In the first setup (depicted in Figure 7.7) users were asked to assess the accuracy of the transformed images (second row) by comparing them with non-deformed reference images (first row). They scrolled through the deformed slices, mainly focusing on the coronal plane. After an initial evaluation, we introduced the additional green reference line and gathered feedback on its usefulness.

Feedback

The following themes emerged from the think-aloud protocol, combined with the interview questions for this first setup. In this initial image-layout all planes (axial, coronal and sagittal) were shown (see Figure 7.7), but participants immediately pointed out that only the coronal view (middle column) was useful for the flattened volume, as they would always refer back to the original image for the axial view. The coronal perspective was highlighted by all participants for providing a clear and efficient overview. The
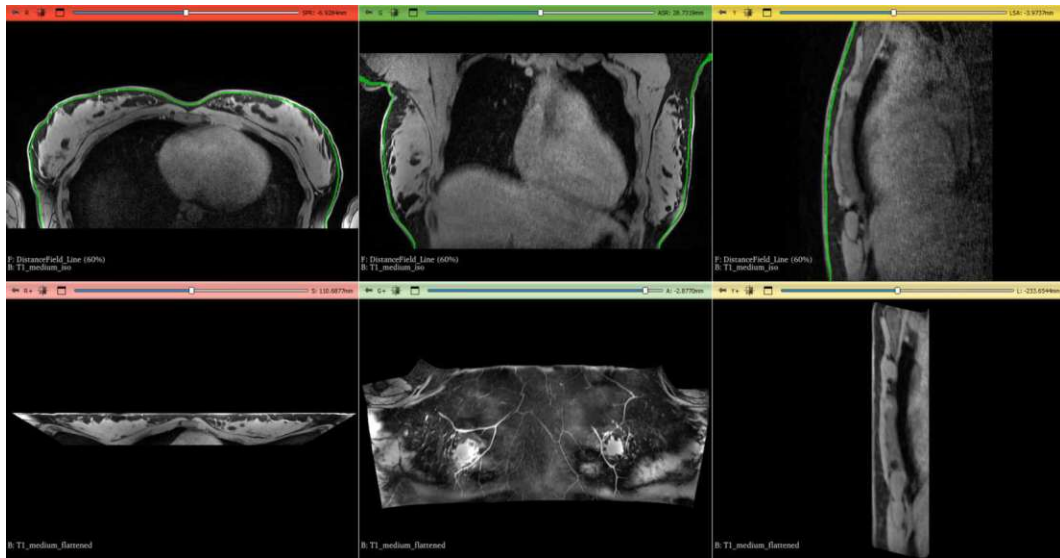
Figure 7.7: Setup 1: Demonstration of the surface-cutting approach. The original images in the first row, the deformed image in the second, each in axial, coronal and sagittal views.

interviewees found the visualization to be well-aligned with clinical practice, particularly in aiding real-world applications. One radiologist noted: *"The coronal view is great, it makes so much more sense than the original [. . .] it is particularly important for the clinical workflow, especially for identifying a lesion during a biopsy."* Two participants positively highlighted the vessel visualization, noting that the vessels are clearly visible in a single plane. All participants noted that the system is intuitive and easy to navigate, with radiologists highlighting that their expertise allows for a seamless linkage to original images: *"It's absolutely intuitive; every radiologist should know where this is."* The detection of potential lesion was also considered effective, with no major concerns about missing small abnormalities. Additionally, users reported minimal visual distortions, noting that any initial perception of distortion would quickly fade with experience.

In a second step, the navigation aid in form of a green reference line to the original image was demonstrated. Participants appreciated the feature and found it helpful for orientation, especially in larger breasts. One participant described it as *"very aesthetic and practical"*. One radiologists noted that while the feature could be particularly useful for users less familiar with the visualization, its frequency of use would likely vary depending on the radiologists' preferences.

7.2.3   Setup 2: Landmark Warp Approach

Similar to the first setup, this setup (depicted in Figure 7.8) provided an introduction to the second approach. Here, we applied the landmark warp to the same T1-weighted medium-sized breast dataset. Participants were again encouraged to think aloud while

exploring the visualization. After their initial impressions, we demonstrated the additional features, showing the deformation grid, placing synced annotations and measurement of lesions. Here again all participants scrolled through the slices and mainly put their focus on the coronal plane. Based on feedback from medical physics experts, we additionally presented a non-masked version of the prototype (see Figure 7.9) in subsequent interviews with radiologists to ensure that the masking did not influence the participants' overall impression of the visualization.
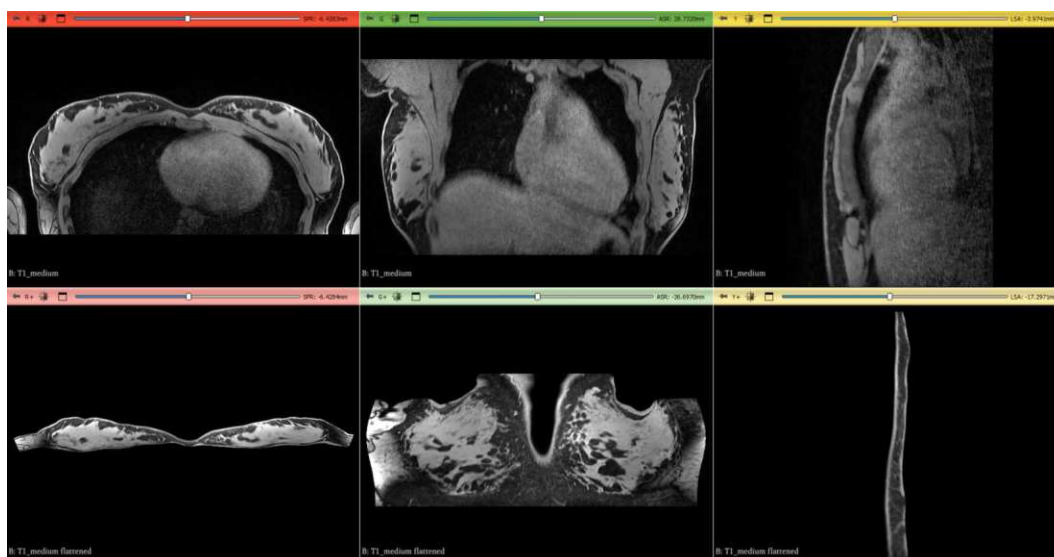
Figure 7.8: Setup 2: Demonstration of the landmark warp approach. The original images in the first row, the deformed image in the second, each in axial, coronal and sagittal views.
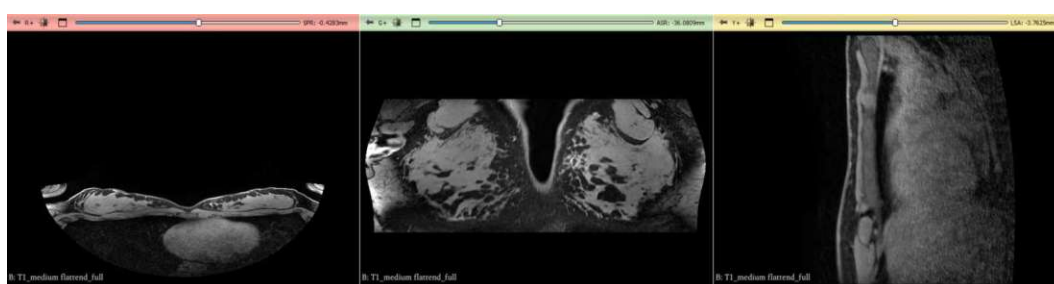
Figure 7.9: Setup 2: Demonstration of the landmark warp approach, non-masked version.

Feedback

Participants found it easy to link to the original images, with no significant changes compared to the first approach. The axial view was particularly appreciated for its clearer spatial orientation, one participant explained, *"In the axial view, spatial orientation is*

clearer — I can immediately recognize and imagine how it was unfolded." For the second approach, especially when focused on the coronal view, the participants found it less intuitive. One participant stated, *"My gut feeling tells me that orientation was easier in the first version"*. Still, none of the radiologists reported difficulties in establishing correspondence to the original images. One noted: *"It needs time to get used to, but there is no need of explanation"*. Radiologists and domain experts noted that it appeared more anatomically accurate and less distorted. Even though the axial view was considered more natural by three participants, all participant expressed preference for the first approach for its overview and ease of orientation, especially when considering the coronal view. Participants also raised concerns regarding landmark visibility in the second approach, particularly due to the masked presentation of surrounding structures. The removal of the rib cage was seen as reducing important anatomical references, making it harder to assess cases where tumors may infiltrate the chest wall (see difference in Figure 7.8 compared to Figure 7.9) Additionally, two interviewees noted that vessel visualization was less intuitive in this approach. One participant commented: *"I can trace the blood vessels, but they are not visible in one glance."*

The navigation aids introduced in this setup were again demonstrated. Here especially the annotation feature was highly appreciated in order to mark areas of interest and have a direct linkage between original and deformed visualization. One participant noted: *"This is a great feature — this is very, very good if I look at a lesion in the deformed volume and want to find it in the original again."* Another considered annotations to be even more important than the reference line for accurate communication. The deformation field was considered a "nice-to-have" feature rather than essential for navigation. However, it was seen as useful tool for checking if anything went wrong during the deformation process. The lesion measurement feature was generally seen positively, for example for tasks like chemotherapy assessments. However, opinions on its usage were divided between the two radiologists, with one finding it important, while the other felt annotations might suffice.

7.2.4 Setup 3: Direct Comparison Using Patient Data

In a setting as realistic as possible, radiologists were asked to analyze images containing pathology, closely mirroring their usual diagnostic workflow. Multiple sequences were combined into a "hanging protocol," as depicted in Figure 7.10 and Figure 7.11. The images were arranged as follows: on the left top, the T2-weighted axial non-deformed image was displayed as a reference, followed by five coronal, flattened views in the order: first row - T1 post-contrast, calc B; second row - T2-weighted, T1 subtracted. The focus on the coronal plane responds to Feature F4 in the Requirements (see Table 4.1), and the inclusion of the axial reference view also reflects Feature F2, addressing the need for a seamless switch between original and reformatted images. Additionally, we used a slab MIP for the T1-subtracted sequence, supporting the requested Feature F3. Participants navigated through the slices and zoomed in to closely inspect the pathologies, examining multiple flattened sequences for a thorough analysis. Based on their interactions and responses to interview questions, the following themes were identified.
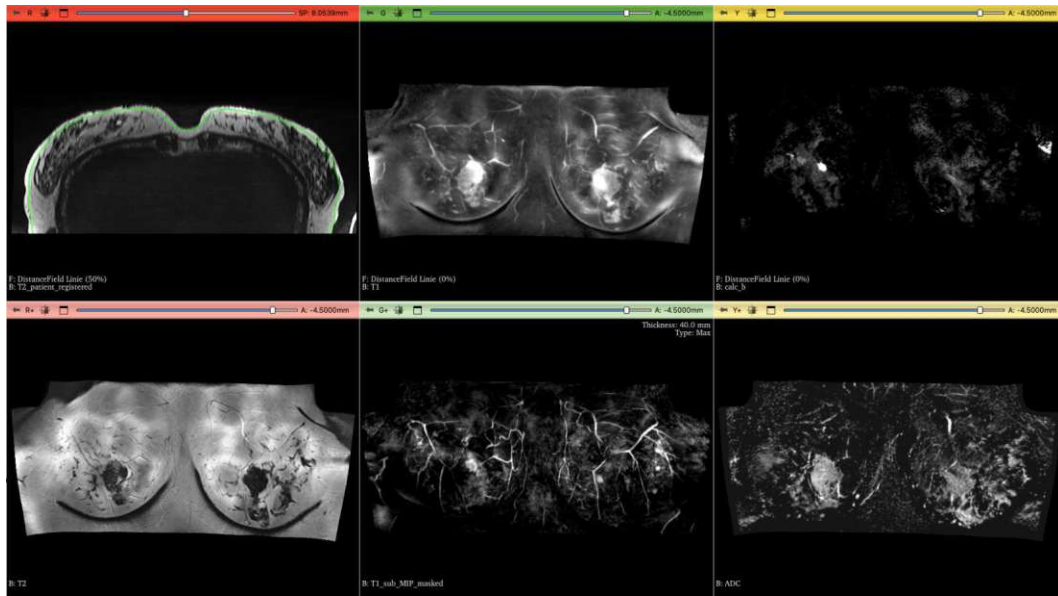
Figure 7.10: Setup 3.1: Evaluation of the surface-cutting approach. Hanging protocol composed of a T2 axial reference (the top left), while the remaining five panels showed coronal flattened versions of different sequences (T1 post-contrast, calc B, T2-weighted, T1 subtracted, and ADC).
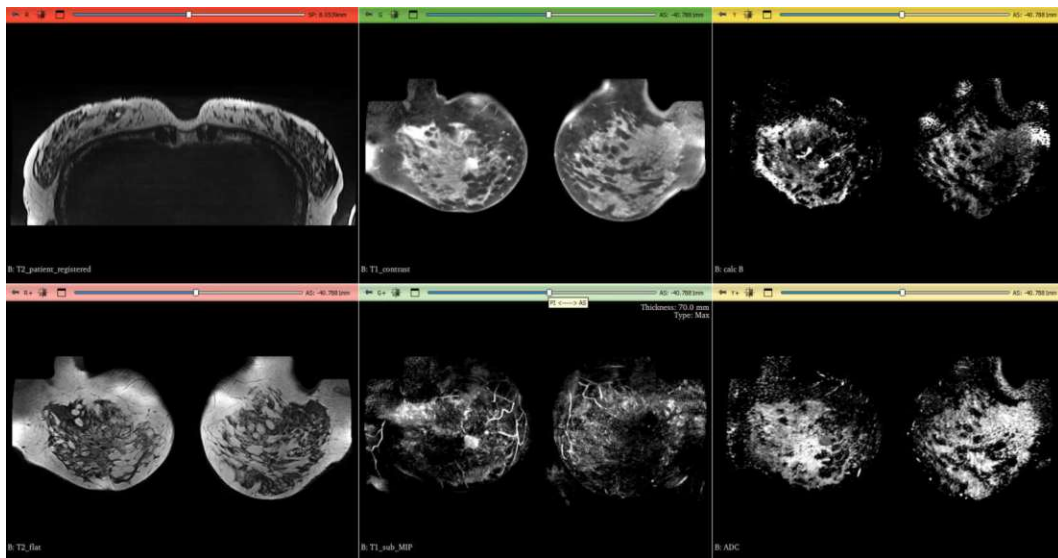
Figure 7.11: Setup 3.2: Evaluation of the landmark warp approach, using the same hanging protocol as in Setup 3.1.

Feedback

Despite their initial preference for the surface-cutting approach due to its intuitive spatial overview, in direct comparison radiologists found the second approach diagnostically

superior when performing actual evaluations. One radiologist noted, *"It's funny—I generally prefer the first version, but diagnostically, the other one is better. I feel like I can orient myself better and assess the volume more effectively"*. The second radiologist commented, *"In direct comparison, I always found this one (approach 2) better"*. The participants still noted that the approach 1 unfolded more intuitive for surface anatomy, particularly around the nipple and vessels. In general, participants confirmed that both approaches allowed for time savings as having fewer images to review results in quicker evaluations. One radiologist highlighted, that the reduced number of images makes it easier to avoid errors.

Across all three setups, a progression in user preferences emerged. In Setup 1, participants appreciated the intuitive spatial overview provided by the first approach, particularly for surface anatomy and vessel visualization. In Setup 2, while the deformation was seen as more natural and anatomically correct, participants still preferred the first approach for general overview. Finally, in Setup 3, which involved side-by-side comparison using pathological cases, radiologists acknowledged the second approach as more diagnostically effective, even if the first version remained more intuitive at a glance. Across all setups, participants emphasized the benefits of a reduced image count, faster interpretation, and the importance of preserving full anatomical context by avoiding masked regions.

7.2.5 Practical Considerations and Adoption

Finally, after evaluating the setups, the interviewees were asked additional interview questions around practical considerations and adoption.

Flat Visualization Supports Adoption of Supine MRI

Participants acknowledged that adopting supine breast MRI and new visualization techniques would take time. A frequently repeated theme was that many radiologists are conservative, particularly with established techniques like the axial view, which they have used for years. While adjusting to the new visualization will take time, participants agreed that this technology could be crucial for widespread use. One imaging expert suggested that it will take a larger quantitative study for assessing reading times and accuracy in order to understanding how quickly users can adapt and how it affects workflow. One radiologist noted that adjusting to new views might be challenging initially, but highlighted the time saving of new visualizations could help the adoption. The second interviewed radiologists emphasized the importance of the demonstrated flat visualizations for supine breast MRI, stating: ***"I honestly think it will only enable its use. Without it, it will never be adopted, never. I'm absolutely sure about that. It's extremely good."***

Need for Flat Visualization

Generally, there was strong support for the flat visualization among participants, especially for smaller breasts, where axial views provide limited information. Despite the challenges

of introducing a new approach, participants felt that over time, the integration of supine breast MRI with axial and flattened views would benefit the process. One participant suggested that this visualization could even enhance current mammography methods.

Acceptable Duration

Participants were also asked about their opinions on acceptable duration for deformation modeling. One radiologist indicated that a processing time of up to five minutes would be acceptable, as it would not disrupt the workflow. Another participant suggested that if deformation took up to 30 minutes, it would be fine as long as the result was available when the radiologists start their diagnosis processes. However, for clinical settings with a quicker pace, such as private hospitals, they emphasized the importance of minimizing delays. Participants noted that the deformation process would need to occur automatically or at least semi-automated, with radiologic technologists reviewing the result as an intermediate step, ensuring a smooth integration into the workflow.

7.2.6 Future Directions and Suggested Improvements

Participants provided several suggestions for improving the visualizations. One radiologist suggested incorporating sagittal views, noting that while the current setup is focused on the coronal view, sagittal views could offer important insights, especially because this is similar to how radiologists work with mammography images. Additionally, the annotation feature available in the second approach, allowing users to click on a specific spot in the visualization and quickly jump to the corresponding location on the original image, was also proposed for the first approach. This would offering radiologists the ability to cross-reference easily. Multiple participants noted the importance of improving the correction for bias field artifacts, such as reducing the visibility of coil artifacts and addressing inhomogeneities in fat suppression. To provide additional confirmation, one imaging expert suggested displaying a distortion field overlay, which would allow radiologists to visualize areas of distortion and feel more confident about the accuracy of the images. Radiologists also recommended adding color overlays for lesion identification, suggesting that color coding could help with quicker and more intuitive lesion detection. This could be implemented as a one-click feature to highlight lesions in different stages, such as washout or plateau.

CHAPTER **8**

Conclusion

8.1 Summary

The goal of this thesis was to develop and evaluate a flattened breast visualization method specifically for supine MRI to enhance its clinical utility. A key challenge in supine breast MRI is that the images results in a thinner axial cross-section due to the distribution of breast tissue over the chest wall, which makes interpretation more difficult [43].

To address this challenge, the following research question was formulated: *To what extent can a flattening-based visualization method improve the clinical utility of supine breast MRI?* We demonstrate in this work that flattening-based visualizations show significant potential to enhance clinical utility of supine MRI by reducing the number of slices radiologists need to review and offering intuitive overviews. We developed two novel visualization prototypes, both designed to "flatten" the breast tissue. These new visualizations are not intended to replace standard views but rather to serve as an initial overview. Following a user-centered design process these prototypes were implemented and evaluated with radiologists and medical physics experts to assess their utility in a diagnostic process. Figure 8.1 summarizes the results from both approaches.

The first prototype employs a surface-cutting approach, starting with a surface mesh based on the segmentation of the breast tissue. It uses an Euclidean distance field and offsets the surface at discrete distances. Each offset mesh is flattened individually using ARAP parameterization and aligned using Procrustes analysis and PCA. This surface-cutting approach builds upon the work of Miao et al. [40], however instead of using mean-value coordinates [22], we employ ARAP parameterization [34, 35]. Additionally, while their method was designed for placenta flattening, our approach addresses the unique challenges of a breast structure, where the surface has complex curvature variations, including concave and convex regions. This first approach was highlighted by radiologists for providing an intuitive overview with clear vessel visualization. Also, the surface mesh

65
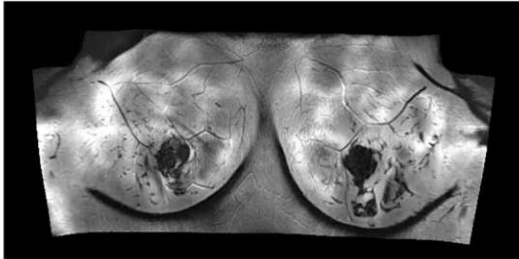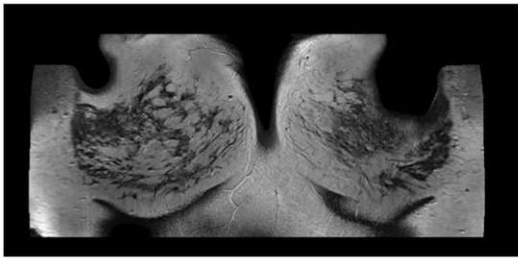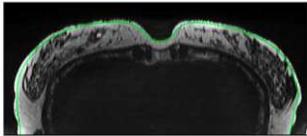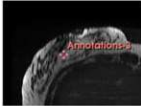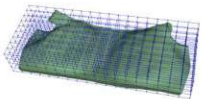
	Approach 1	Approach 2
Result (Coronal)		
Method	**Surface Cutting** • Creation of offset-surfaces through Euclidean distance field • Flattening of each individual offset-surface through ARAP parameterization • Procrustes Analysis and PCA to align flat meshes • Voxelize meshes to volume	**Landmark Warp** • Extraction of curves through segmentation along the ribcage • Flattening of the curves to average arc length • Discretizing control points along curve • TPS Transform with source and target points
Features	• Reference line indicating slice position	• Annotations • Deformation grid
Distortion	• Distortion increases with breast size • 4.4% avg area distortion for medium breast size surface mesh	• Distortion increases with breast size • 10.1% avg area distortion for medium breast size surface mesh • 2.6% avg distance distortion over volume
User Feedback	⊕ • Time savings • Fewer images -> error reduction • Lesion detection intuitive • Easy linkage to original images • Good vessel visualization • Presents a good spatial overview • Well-aligned with clinical practice • Intuitive surface anatomy ⊖ Volumetric distortion during diagnosis	⊕ • Time savings • Fewer images -> error reduction • Lesion detection intuitive • Easy linkage to original images • Axial view more natural • Appears anatomically more accurate and less distorted • Annotations • Preferred for lesion inspection ⊖ • Slightly harder to orient initially • Masked surrounding structures • Vessel visualization less intuitive

Figure 8.1: Overview of the two proposed breast flattening visualization methods and their evaluation results.

exhibited less metric and area distortion — ranging between average values of 2.1% to 3.5% for the metric distortion and 3.7% and 5.8% for the areal distortion. However, one limitation of this approach is the independent flattening of each slice, which potentially distorts depth image information across layers. Therefore inter-layer continuity can not be guaranteed when scrolling through the slices. This is addressed by the second approach, a landmark warp, which operates on the entire volume at once, ensuring better consistency across slices. Our landmark warp approach extends the work of Obermann et al. [43] by automating control point placement and using a landmark warp, within a TPS framework, rather than relying on CPR. The second approach therefore enables direct integration with annotations and measurements, and demonstrated faster processing times (0.5–5.5 minutes). These times align closely with the acceptable range specified by interview participants, who noted processing times of up to five or even 30 minutes would be acceptable, as long as the results were available when they began their diagnostic process. The distortions measured on the mesh surface are higher for the landmark warp approach compared to the first method, with the area distortion ranging from 5.7% to 15.5% increasing with breast size. The volumetric distortion across the whole breast, was relative low with an average between 1.3% to 4.4% depending on breast size.

During the qualitative evaluation, radiologists initially favored the first approach for its intuitive coronal view. However, when examining real patient data, there was a slight preference the second approach due to its superior anatomical correctness. Overall, feedback was very positive for both prototypes, emphasizing the importance of such visualizations to support the clinical adoption of supine breast MRI.

8.2   Limitations and Future Work

One major limitation of the first approach in its current state is processing time. Especially using a dense mesh, the method requires extensive processing, taking approximately 65 minutes for 50 meshes sampled at 1mm intervals. We have shown that these processing times can be significantly reduced to about 1 second per mesh if a sparser mesh is used. However, this also resulted in higher distortions and the impact on lesion visibility and overall accuracy has yet to be evaluated. Despite the time reductions, the mesh extraction and processing is a step that we in general expect to be more time consuming than deforming the entire volume at once. Furthermore, also processing times for the first approach could be reduced, as optimization was not the primary focus of this thesis. Future work could explore potential speed-ups through GPU acceleration or parallelization, which may benefit both approaches.

Another limitation of both methods is the reliance on manual pre-processing steps, described in Section 5.2. The current prototypes for the scope of this thesis depend on manual segmentation and registration. uture work could focus on fully automating these steps in order to improve improving efficiency.

An additional limitation of this study is the small number of participants involved in the qualitative evaluations. Both the requirements gathering and the final evaluation

were conducted with the same four individuals. While re-engaging the same participants allowed us to directly assess how well the visualizations addressed their needs, it potentially comes at cost of generalizability of the findings. For future work, a larger quantitative evaluation could help to assess the effectiveness of visualizations. Such studies could investigate their impact on diagnostic accuracy, reading times, and user adaptation, providing a more comprehensive understanding of their clinical value. Additionally, while this study has focused on supine imaging, similar visualization methods could be adapted for prone breast MRI, as raised by the radiologists in relation to the vessel visualization.

Despite these limitations, the results presented here demonstrate significant potential for flattening-based visualization methods to enhance the clinical utility of supine breast MRI. This research lays the foundation for further refinement and, ultimately, the broader adoption of supine breast MRI in clinical practice.

APPENDIX A

Interview Guide (Expert)

This appendix contains the interview guide used during the initial semi-structured interviews with medical physics experts.

Part I: Introduction

- *Welcome and introduction*
- *Brief explanation of the master's thesis: "Flattening-Based Visualization of Supine Breast MRI"*
- *Clarification of the interview's purpose*
- *Mention of estimated interview duration (about one hour)*
- *Confirmation of consent to record the interview*

General Questions

- Could you briefly describe your professional background and experience in medical physics?
- How long have you been working with breast MRI hardware?

Part II: Hardware and Image Acquisition

Hardware Development

- Could you describe the developed hardware (BraCoil) for supine breast MRIs?

69

- How is the hardware applied in practice?

- What specific requirements and considerations went into the development?

Image Acquisition

- Could you describe the image acquisition process for supine breast MRIs?

  – What sequences are typically used?

  – How do techniques vary with and without contrast agents?

- What differences and challenges exist between prone and supine imaging (e.g., motion)?

Part III: Panoramic Visualization

Visualization of Supine Breast MRIs

- What were the main goals in developing this visualization?

- How do visualizations of supine breast MRIs differ from prone ones?

- Could you briefly explain how the current "panoramic visualization" is generated?

  – Which manual steps are involved in creating the visualization?

- What insights has the visualization already provided?

- What limitations have you observed in the current panoramic visualization?

Application of Panoramic Visualization

- What features and functionalities would you want in an ideal panoramic visualization?

- What tasks would you like to perform with it?

- Are there specific clinical scenarios where the panoramic visualization is particularly useful or not useful?

- Have you received any feedback from end-users?

Part IV: Deformation Demo

Parameterization and Distortions

- Suppose we have the following breast MRI image (printed axial supine MRI slice), could you please indicate how you would deform it?

- We would like to show you several possible deformation mock-ups (see Figure A.1, A.2, A.4) and like to hear your opinion.
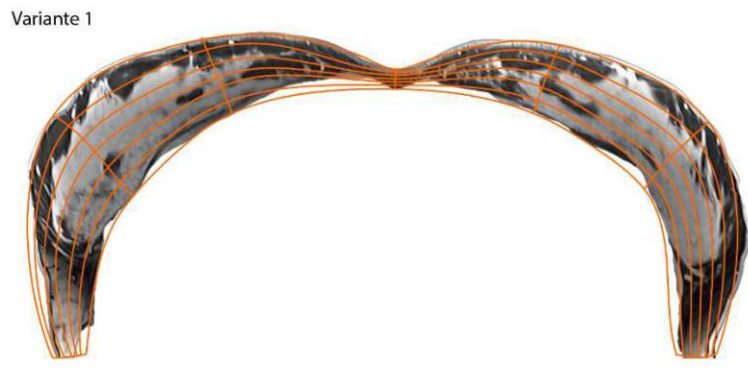
Figure A.1: Mock-Up Version 1
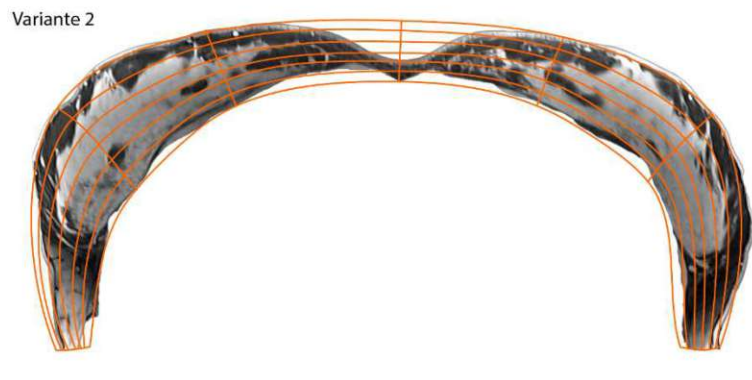
Figure A.2: Mock-Up Version 2
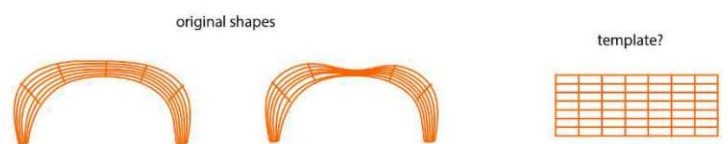
Figure A.3: Deformation of Version 1 and Version 2

Figure A.4: Mock-Up Version 3

Figure A.5: Deformation of Version 3

Feedback on Techniques

- What do you think of these techniques?

- Which technique do you find most useful, and why?

- Are there distortions you find particularly problematic (e.g., between the breasts or at the edges under the arms)?

- Do you have suggestions to improve or adapt these techniques?

- Should differences in breast size be reflected in the flattened visualization?

- Can the breasts be considered separately, or is it important to have a continuous visualization?

Part V: Closing Questions

- Are there any other aspects or challenges of supine breast MRI we haven't discussed that you consider important?

- Would you like to add anything or ask us questions?

Debriefing

- *Thank participant for their time and valuable insights. Inform them about the further course of the project and how the interview results will be used.*

APPENDIX B

Interview Guide (User)

This appendix contains the interview guide used during the initial semi-structured interviews with radiologists.

Part I: Introduction

- *Welcome and introduction*

- *Brief explanation of the master's thesis: "Flattening-Based Visualization of Supine Breast MRI"*

- *Clarification of the interview's purpose*

- *Mention of estimated interview duration (about one hour)*

- *Confirmation of consent to record the interview*

General Questions

- Could you please briefly describe your professional background and your experience in radiology?

- How long have you been working in radiology?

Part II: Diagnostic Workflow

- Could you describe the MRI image acquisition workflow and protocol (sequences, use of contrast agents)?

- How does the diagnosis process for breast MRIs work in practice?

- Could you show me how you typically analyze an MRI image? (preferably demo in 3D Slicer)

- How do you proceed with lesion detection in breast MRIs?

- What specific features (landmarks) or patterns do you examine when analyzing the images?

- Are there specific areas of the breast that require particular attention?

- Are there current challenges you face in lesion detection?

- What tools do you currently use for lesion detection? What limitations and aspects for improvement do you see?

Part III: Supine Breast MRIs

Supine Breast MRIs:

- What differences do you see in interpreting breast MRIs in the supine versus prone (lying on the stomach) position?

- Are there specific advantages or disadvantages that you notice with the supine position?

Visualization Requirements:

- If you could imagine an "ideal visualization" for supine breast MRIs, what information should be included to detect lesions most effectively?

- In your opinion, what would be the minimum distance between MRI slices that is necessary (1mm, 2mm, 3mm...)?

Part IV: Image Parametrization Demo

Parametrization and Distortions:

- Suppose we have the following breast MRI image (printed axial supine MRI slice), could you please indicate how you would deform it?

- We would like to show you several possible deformation mock-ups (see Figure B.1, B.2, B.4) and like to hear your opinion.

Figure B.1: Mock-Up Version 1
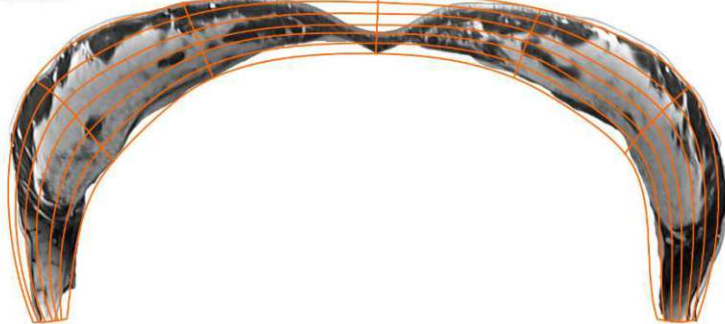
Figure B.2: Mock-Up Version 2
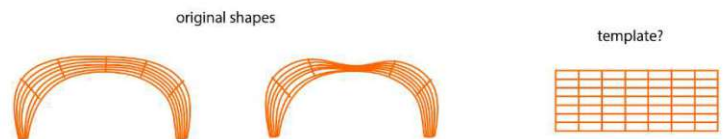
Figure B.3: Deformation of Version 1 and Version 2

Feedback on Techniques:

- What do you think of these techniques?

- Do you find these techniques helpful? If yes, why?

- Are there any specific distortions that you find problematic (e.g., between the breasts or at the edges under the arms)?

- Do you have any suggestions for improving or adapting these parametrization approaches?
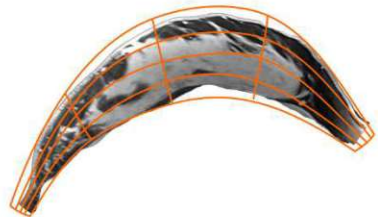
Figure B.4: Mock-Up Version 3
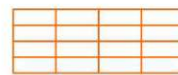
Figure B.5: Deformation of Version 3

- Do you think a size difference between the breasts should also be reflected in the "flattened" visualization?

- Can the breasts be considered separately, or is it important to have a continuous visualization?

Part V: Closing Questions

- Are there any other aspects or challenges of supine breast MRI we haven't discussed that you consider important?

- Would you like to add anything or ask us questions?

Debriefing

- *Thank participant for their time and valuable insights. Inform them about the further course of the project and how the interview results will be used.*

Evaluation: Interview Guide

Part I: Introduction

- *Welcome and introduction*

- *Explain the purpose of the interview: I will show you two different visualizations of supine breast MRIs. I ask you to speak out everything that catches your attention during the interview. Imagine it is part of a real diagnostic process and feel free to say anything that comes to mind. There are no right or wrong answers. We are interested in how helpful these visualizations would be for your work and what aspects we could possibly improve.*

- *Note on the duration of the interview (approximately one hour)*

- *Confirmation of consent to record the interview and screen*

Part II: Slicer Demo

Setup 1: Surface Flattening Approach

Description: This involves deforming the breast based on the breast surface and corresponding offset-surfaces.

Distortion

1. To what extent can you identify important anatomical structures and potential lesions in the visualization?

2. Do you see distortions in the visualization? If so, in which areas are they most pronounced?

3. How much do these distortions affect your ability to reliably detect lesions?

Effort / Navigation

1. How intuitive is the navigation in the flattened visualization? Are there specific aspects of the visualization that need further explanation or seem unfamiliar?

2. How well can you link the flattened version with the original visualization?

Diagnosis Workflow

1. How helpful would such a visualization be for daily diagnosis?

2. Do you see potential for time savings compared to traditional methods?

Next: demonstration of the navigation aid (green line).

Navigation Aid

1. To what extent has displaying the "Navigation Aid" improved your spatial orientation within the image?

Setup 2: Landmark Warp Approach

Description: This involves deforming the breast based on specific control points.

Distortion

1. To what extent can you identify important anatomical structures and possible lesions in the visualization?

2. Do you see distortions in the visualization? If so, in which areas are they most pronounced?

3. How much do these distortions affect your ability to reliably detect lesions?

Effort / Navigation

1. How intuitive is the navigation in the flattened visualization? Are there specific aspects of the visualization that need further explanation or seem unfamiliar?

2. How well can you link the flattened version with the original visualization?

Diagnosis Workflow

1. How helpful would such a visualization be for daily diagnosis?

2. Do you see potential for time savings compared to traditional methods?

Next: visualize the deformation grid in form of the control point overlay.

Navigation Aid

1. To what extent has the display of the "Deformation Grid" improved your spatial orientation within the image?

Next: demonstrate the ability of synced annotations.

Annotation Feature

1. How useful did you find the ability to make annotations in the flattened view and transfer them to the original image?

2. How useful did you find the ability to scroll synchronously through both the original and deformed views?

Setup 3: Comparison of both on patient data

1. Did you observe different distortions in the different breast sizes?

2. Which prototype convinced you the most? Why?

3. Were there differences between the visualizations regarding the level of detail or the detectability of small lesions?

4. Which visualization provided the best spatial orientation within the breast?

5. Which of the two visualizations is the most intuitive to interpret for you?

Duration

1. How long would you be willing to wait for a visualization if it would improve its accuracy or functionality?

Clinical Workflow

1. To what extent could one of these visualizations make the use of supine breast MRIs easier or more practical in clinical practice?

2. Which of the visualizations could contribute most to simplifying the clinical workflow (e.g., faster detection of relevant structures, improved clarity)?

3. Do you believe this visualization format could reduce the time required for diagnosis? If yes, to what extent?

4. Could you imagine using one of these visualizations in your daily work?

Features

1. How important is it for you to be able to make annotations or markings directly in the flattened view, which can then be transferred to the original view?

2. How important is it to have a direct link to the original, non-deformed images?

3. How important is it to scroll synchronously between the original and deformed views?

Future Outlook

1. What specific improvements would be required to implement this visualization in your clinical practice?

2. What additional features or representations would you like to see?

Part IV: Conclusion

- Are there any other aspects or challenges we have not discussed that you consider important?

- Would you like to add anything else or have any questions?

Debriefing

- *Thank participant for their time and valuable insights. Inform them about the further course of the project and how the interview results will be used.*

Overview of Generative AI Tools Used

The German versions of the abstract and the questionnaires in the appendix were initially translated using the free version of DeepL and Google Translate. ChatGPT (GPT-3.5 and GPT-4o) was employed to assist with grammar and phrasing. All outputs from these tools required substantial manual revision and adaptation. No AI-generated content was used without significant changes.

List of Figures

List of Tables

Bibliography

[1] 3D Slicer image computing platform. https://slicer.org/. accessed on March 12, 2025.

[2] Breast cancer. https://www.who.int/news-room/fact-sheets/detail/breast-cancer. accessed on March 11, 2025.

[3] The Computational Geometry Algorithms Library. https://www.cgal.org/. accessed on March 17, 2025.

[4] PerkLab/SlicerSandbox. https://github.com/PerkLab/SlicerSandbox. accessed on March 5, 2025.

[5] Pyvista/pyacvd. https://github.com/pyvista/pyacvd. accessed on May 15, 2025.

[6] S. Mazdak Abulnaga, Esra Abaci Turk, Mikhail Bessmeltsev, P. Ellen Grant, Justin Solomon, and Polina Golland. Volumetric Parameterization of the Placenta to a Flattened Template. *IEEE Transactions on Medical Imaging*, 41(4):925–936, April 2022.

[7] Ahlberg. Chapter II The Cubic Spline. In *Mathematics in Science and Engineering*, volume 38, pages 9–74. Elsevier, 1967.

[8] Pascal Andreas Thomas Baltzer, Kathrin Barbara Krug, and Matthias Dietzel. Evidence-Based and Structured Diagnosis in Breast MRI using the Kaiser Score. *RöFo - Fortschritte auf dem Gebiet der Röntgenstrahlen und der bildgebenden Verfahren*, 194:1216–1228, May 2022.

[9] J. Gordon Betts, Kelly A. Young, James A. Wise, Eddie Johnson, Brandon Poe, Dean H. Kruse, Oksana Korol, Jody E. Johnson, Mark Womble, and Peter DeSaix. Anatomical Terminology. In *Anatomy and Physiology 2e*. OpenStax, April 2022.

[10] Ann Blandford. *Semi-Structured Qualitative Studies*. The Encyclopedia of Human-Computer Interaction, 2nd Ed. Interaction Design Foundation (IxDF), 2013.

[11] F. L. Bookstein. Principal Warps: Thin-Plate Splines and the Decomposition of Deformations. *IEEE Trans. Pattern Anal. Mach. Intell.*, 11(6):567–585, June 1989.

[12] Virginia Braun and Victoria Clarke. Using thematic analysis in psychology. *Qualitative Research in Psychology*, 3:77–101, January 2006.

[13] Sheelagh Carpendale. Evaluating Information Visualizations. In Andreas Kerren, John T. Stasko, Jean-Daniel Fekete, and Chris North, editors, *Information Visualization: Human-Centered Issues and Perspectives*, pages 19–45. Springer, Berlin, Heidelberg, 2008.

[14] Paola Clauser, Matthias Dietzel, Michael Weber, Clemens G Kaiser, and Pascal AT Baltzer. Motion artifacts, lesion type, and parenchymal enhancement in breast MRI: What does really influence diagnostic accuracy? *Acta Radiologica*, 60(1):19–27, January 2019.

[15] Per-Erik Danielsson. Euclidean distance mapping. *Computer Graphics and Image Processing*, 14(3):227–248, November 1980.

[16] Matthias Dietzel and Pascal A. T. Baltzer. How to use the Kaiser score as a clinical decision rule for diagnosis in multiparametric breast MRI: A pictorial essay. *Insights into Imaging*, 9(3):325–335, June 2018.

[17] Gianluca Donato and Serge Belongie. Approximation Methods for Thin Plate Spline Mappings and Principal Warps. In *Computer Vision — ECCV 2002*, volume 2352 of *Lecture Notes in Computer Science*, pages 21–31. Springer, Berlin, Heidelberg, 2002.

[18] Ian L. Dryden and Kanti V. Mardia. Procrustes Analysis. In *Statistical Shape Analysis, with Applications in R*, chapter 7, pages 125–173. John Wiley & Sons, Ltd, 2016.

[19] Basak Erguvan-Dogan, Gary J. Whitman, Anne C. Kushwaha, Michael J. Phelps, and Peter J. Dempsey. BI-RADS-MRI: A Primer. *American Journal of Roentgenology*, 187(2):W152–W160, August 2006.

[20] Andriy Fedorov, Reinhard Beichel, Jayashree Kalpathy-Cramer, Julien Finet, Jean-Christophe Fillion-Robin, Sonia Pujol, Christian Bauer, Dominique Jennings, Fiona Fennessy, Milan Sonka, John Buatti, Stephen Aylward, James V. Miller, Steve Pieper, and Ron Kikinis. 3D Slicer as an image computing platform for the Quantitative Imaging Network. *Magnetic Resonance Imaging*, 30(9):1323–1341, November 2012.

[21] Michael S. Floater. Parametrization and smooth approximation of surface triangulations. *Computer Aided Geometric Design*, 14(3):231–250, April 1997.

[22] Michael S. Floater. Mean value coordinates. *Computer Aided Geometric Design*, 20(1):19–27, March 2003.

[23] Francis Fortin. Multiplanar reformation (MPR) | Radiology Reference Article | Radiopaedia.org. https://radiopaedia.org/articles/multiplanar-reformation-mpr, January 2019. accessed on April 16, 2025.

[24] Frank Gaillard. MRI sequences (overview) | Radiology Reference Article | Radiopaedia.org. https://radiopaedia.org/articles/mri-sequences-overview, June 2015. accessed on March 11, 2025.

[25] Eloy García, Yago Diez, Oliver Diaz, Xavier Lladó, Robert Martí, Joan Martí, and Arnau Oliver. A step-by-step review on patient-specific biomechanical finite element models for breast MRI to x-ray mammography registration. *Medical Physics*, 45(1):e6–e31, 2018.

[26] Ophira Ginsburg, Cheng-Har Yip, Ari Brooks, Anna Cabanes, Maira Caleffi, Jorge Dunstan Y., Bishal Gyawali, Valerie McCormack, Myrna McLaughlin de Anderson, Ravi Mehrotra, Alejandro Mohar, Raul Murillo, Lydia E. Pace, Electra D. Paskett, Anya Romanoff, Anne F. Rositch, John Scheel, Miriam Schneidman, Karla Unger-Saldana, Verna Vanderpuye, Tsu-Yin Wu, Safina Yuma, Allison Dvaladze, Catherine Duggan, and Benjamin O. Anderson. Breast cancer early detection: A phased approach to implementation. *Cancer*, 126(Suppl 10):2379–2393, May 2020.

[27] Christo Gnonnou and Nadia Smaoui. Segmentation and 3D reconstruction of MRI images for breast cancer detection. *International Image Processing, Applications and Systems Conference, IPAS 2014*, February 2015.

[28] Nicolas Grossmann, Thomas Köppel, Eduard Gröller, and Renata Georgia Raidou. VisualFlatter - Visual Analysis of Distortions in the Projection of Biomedical Structures. *Eurographics Workshop on Visual Computing for Biology and Medicine*, page 11 pages, 2018.

[29] Hans J Johnson, Matthew M McCormick, and Luis Ibanez. 2.8 Distance Map. In *The ITK Software Guide Book 2: Design and Functionality Fourth Edition*, pages 134–137. Kitware, Inc., May 2024.

[30] A. Kanitsar, D. Fleischmann, R. Wegenkittl, P. Felkel, and E. Groller. CPR - curved planar reformation. In *IEEE Visualization, 2002. VIS 2002.*, pages 37–44, Boston, MA, USA, 2002. IEEE.

[31] R. C. Katz, L. Wilson, and N. Frazer. Anxiety and its determinants in patients undergoing magnetic resonance imaging. *Journal of Behavior Therapy and Experimental Psychiatry*, 25(2):131–134, June 1994.

[32] Stefan Klein, Marius Staring, Keelin Murphy, Max A. Viergever, and Josien P. W. Pluim. Elastix: A toolbox for intensity-based medical image registration. *IEEE transactions on medical imaging*, 29(1):196–205, January 2010.

[33] J. Kreiser, M. Meuschke, G. Mistelbauer, B. Preim, and T. Ropinski. A Survey of Flattening-Based Medical Visualization Techniques. *Computer Graphics Forum*, 37(3):597–624, 2018.

[34] Jan Kretschmer, G. Soza, Christian Tietjen, Michael Suehling, Bernhard Preim, and Marc Stamminger. ADR-Anatomy-driven reformation. *IEEE Transactions on Visualization and Computer Graphics*, 20, November 2014.

[35] Ligang Liu, Lei Zhang, Yin Xu, Craig Gotsman, and Steven J. Gortler. A Local/Global Approach to Mesh Parameterization. *Computer Graphics Forum*, 27(5):1495–1504, July 2008.

[36] William E. Lorensen and Harvey E. Cline. Marching cubes: A high resolution 3D surface construction algorithm. In *Proceedings of the 14th Annual Conference on Computer Graphics and Interactive Techniques*, SIGGRAPH '87, pages 163–169, New York, NY, USA, August 1987. Association for Computing Machinery.

[37] R. M. Mann, C. K. Kuhl, K. Kinkel, and C. Boetes. Breast MRI: Guidelines from the European Society of Breast Imaging. *European Radiology*, 18(7):1307–1318, July 2008.

[38] Ritse M. Mann, Corinne Balleyguier, Pascal A. Baltzer, Ulrich Bick, Catherine Colin, Eleanor Cornford, Andrew Evans, Eva Fallenberg, Gabor Forrai, Michael H. Fuchsjäger, Fiona J. Gilbert, Thomas H. Helbich, Sylvia H. Heywang-Köbrunner, Julia Camps-Herrero, Christiane K. Kuhl, Laura Martincich, Federica Pediconi, Pietro Panizza, Luis J. Pina, Ruud M. Pijnappel, Katja Pinker-Domenig, Per Skaane, Francesco Sardanelli, and with language review by Europa Donna-The European Breast Cancer Coalition for the European Society of Breast Imaging (EU-SOBI). Breast MRI: EUSOBI recommendations for women's information. *European Radiology*, 25(12):3669–3678, December 2015.

[39] Ritse M. Mann, Nariya Cho, and Linda Moy. Breast MRI: State of the Art. *Radiology*, 292(3):520–536, September 2019.

[40] Haichao Miao, Gabriel Mistelbauer, Alexey Karimov, Amir Alansary, Alice Davidson, David F. A. Lloyd, Mellisa Damodaram, Lisa Story, Jana Hutter, Joseph V. Hajnal, Mary Rutherford, Bernhard Preim, Bernhard Kainz, and M. Eduard Groller. Placenta Maps: In Utero Placental Health Assessment of the Human Fetus. *IEEE Transactions on Visualization and Computer Graphics*, 23(6):1612–1623, June 2017.

[41] Lena Nohava, Paola Clauser, Raphaela Czerny, Pascal A. T. Baltzer, and Elmar Laistler. Supine breast MRI using a wearable coil facilitates the translation of MR imaging findings to clinical practice. *European Journal of Radiology*, 184, March 2025.

[42] Lena Nohava, Raphaela Czerny, Martin Tik, Dagmar Wurzer, Elmar Laistler, and Roberta Frass-Kriegl. Citizen science approach to assessing patient perception of MRI with flexible radiofrequency coils. *Scientific Reports*, 14(1):2811, February 2024.

94

[43] Michael Obermann, Lena Nohava, Roberta Frass-Kriegl, Onisim Soanca, Jean-Christophe Ginefri, Jacques Felblinger, Paola Clauser, Pascal Baltzer, and Elmar Laistler. Panoramic Magnetic Resonance Imaging of the Breast With a Wearable Coil Vest. *Investigative radiology*, Publish Ahead of Print, May 2023.

[44] PDQ Screening and Prevention Editorial Board. PDQ Breast Cancer Screening. https://www.cancer.gov/types/breast/patient/breast-screening-pdq, February 2025. accessed March 10, 2025.

[45] Katja Pinker, Roberto Lo Gullo, Janice S. Sung, and Christopher Comstock. Chapter 4 - Standard terminology and reporting– Breast Imaging Reporting & Data System: Magnetic resonance imaging. In Katja Pinker, Ritse Mann, and Savannah Partridge, editors, *Advances in Magnetic Resonance Technology and Applications*, volume 5 of *Breast MRI*, pages 49–63. Academic Press, January 2022.

[46] Csaba Pinter, Andras Lasso, and Gabor Fichtinger. Polymorph segmentation representation for medical image computing. *Computer Methods and Programs in Biomedicine*, 171:19–26, April 2019.

[47] Csaba Pinter, Andras Lasso, An Wang, David Jaffray, and Gabor Fichtinger. SlicerRT: Radiation therapy research toolkit for 3D Slicer. *Medical Physics*, 39(10):6332–6338, 2012.

[48] Bernhard Preim and Charl Botha. Chapter 03 - An Introduction to Medical Visualization in Clinical Practice. In *Visual Computing for Medicine (Second Edition)*, pages 69–110. Morgan Kaufmann, Boston, January 2014.

[49] Bernhard Preim and Charl Botha. Chapter 11 - Visualization of Vascular Structures. In *Visual Computing for Medicine (Second Edition)*, pages 401–449. Morgan Kaufmann, Boston, January 2014.

[50] Bernhard Preim and Charl Botha. Chapter e14 - Projections and Reformations. In *Visual Computing for Medicine (Second Edition)*, pages e1–e17. Morgan Kaufmann, Boston, January 2014.

[51] Bernhard Preim, Timo Ropinski, and Petra Isenberg. A Critical Analysis of the Evaluation Practice in Medical Visualization. *Eurographics Workshop on Visual Computing for Biology and Medicine*, page 12 pages, 2018.

[52] Jeremy Price. Basics of breast MRI. In *Handbook of Breast MRI*, pages 1–21. Cambridge University Press, 1 edition, November 2011.

[53] Jeremy Price. Imaging-related anatomy and pathology. In *Handbook of Breast MRI*, pages 22–48. Cambridge University Press, 1 edition, November 2011.

[54] Leonhard Rist, Pluvio Stephan, Noah Maul, Linda Vorberg, Hendrik Ditt, Michael Sühling, Andreas Maier, Bernhard Egger, and Oliver Taubmann. Neural Image

Unfolding: Flattening Sparse Anatomical Structures using Neural Fields, November 2024.

[55] Karl Rohr and Stefan Wörz. An extension of thin-plate splines for image registration with radial basis functions. In *2012 9th IEEE International Symposium on Biomedical Imaging (ISBI)*, pages 442–445, May 2012.

[56] Will Schroeder, Ken Martin, and Bill Lorensen. *The Visualization Toolkit (4th Ed.).* Kitware, 2006.

[57] Denis P. Shamonin, Esther E. Bron, Boudewijn P. F. Lelieveldt, Marion Smits, Stefan Klein, Marius Staring, and Alzheimer's Disease Neuroimaging Initiative. Fast parallel image registration on CPU and GPU for diagnostic classification of Alzheimer's disease. *Frontiers in Neuroinformatics*, 7:50, 2013.

[58] Ewan Simpson, Savvas Andronikou, Schadie Vedajallam, Anith Chacko, and Ngoc Jade Thai. Curved reformat of the paediatric brain MRI into a 'flat-earth map' — standardised method for demonstrating cortical surface atrophy resulting from hypoxic–ischaemic encephalopathy. *Pediatric Radiology*, 46(10):1482–1488, September 2016.

[59] M Smolik and V Skala. Vector Field Interpolation with Radial Basis Functions. *SIGRAD*, pages pp. 127–003, May 2016.

[60] J. Souza, M. J. S. Maciel, E. F. Marques, M. Poli, L. Graziano, and D. S. GIRAO. Breast Lymphoma: A pictorial review. https://epos.myesr.org/poster/esr/ecr2012/C-1770, March 2012.

[61] C. Bane Sullivan and Alexander A. Kaszynski. PyVista: 3D plotting and mesh analysis through a streamlined interface for the Visualization Toolkit (VTK). *Journal of Open Source Software*, 4(37):1450, May 2019.

[62] Hyuna Sung, Jacques Ferlay, Rebecca L. Siegel, Mathieu Laversanne, Isabelle Soerjomataram, Ahmedin Jemal, and Freddie Bray. Global Cancer Statistics 2020: GLOBOCAN Estimates of Incidence and Mortality Worldwide for 36 Cancers in 185 Countries. *CA: A Cancer Journal for Clinicians*, 71(3):209–249, 2021.

[63] Abdel Aziz Taha and Allan Hanbury. Metrics for evaluating 3D medical image segmentation: Analysis, selection, and tool. *BMC Medical Imaging*, 15(1):29, August 2015.

[64] I. Thomassin-Naggara, I. Trop, L. Lalonde, J. David, L. Péloquin, and J. Chopier. Tips and techniques in breast MRI. *Diagnostic and Interventional Imaging*, 93(11):828–839, November 2012.

[65] Thorsten Twellmann, Anke Meyer-Baese, Oliver Lange, Simon Foo, and Tim W. Nattkemper. Model-free visualization of suspicious lesions in breast MRI based

on supervised and unsupervised learning. *Engineering Applications of Artificial Intelligence*, 21(2):129–140, March 2008.

[66] Hafiz Zia Ur Rehman and Sungon Lee. Automatic Image Alignment Using Principal Component Analysis. *IEEE Access*, 6:72063–72072, 2018.

[67] Sébastien Valette and Jean-Marc Chassery. Approximated Centroidal Voronoi Diagrams for Uniform Polygonal Mesh Coarsening | Request PDF. *ResearchGate*, December 2024.

[68] Stéfan van der Walt, Johannes L. Schönberger, Juan Nunez-Iglesias, François Boulogne, Joshua D. Warner, Neil Yager, Emmanuelle Gouillart, and Tony Yu. Scikit-image: Image processing in Python. *PeerJ*, 2:e453, June 2014.

[69] Lulu Wang. Early Diagnosis of Breast Cancer. *Sensors*, 17(7):1572, July 2017.

[70] Huabing Zhou, Yuyu Kuang, Zhenghong Yu, Shiqiang Ren, Anna Dai, Yanduo Zhang, Tao Lu, and Jiayi Ma. Non-rigid image deformation algorithm based on MRLS-TPS. In *2017 IEEE International Conference on Image Processing (ICIP)*, pages 2269–2273, September 2017.